ECS Journal of Solid State
Science and Technology



OPEN ACCESS

# Review—Reliability and Degradation Mechanisms of Deep UV AlGaN LEDs

To cite this article: Benjamin C. Letson *et al* 2023 *ECS J. Solid State Sci. Technol.* **12** 066002

*ECS Journal of Solid State Science and Technology*, 2023 **12** 066002

# Review—Reliability and Degradation Mechanisms of Deep UV AlGaN LEDs

**Benjamin C. Letson,[1] John W. Conklin,[1] Peter Wass,[1] Simon Barke,[2] Guido Mueller,[2] Md Abu Jafar Rasel,[3] Aman Haque,[3] Stephen J. Pearton,[4,z,*] and Fan Ren[5,*]**

[1]*Department of Mechanical and Aerospace Engineering, University of Florida, Gainesville Florida 32611 United States of America*
[2]*Department of Physics, University of Florida, Gainesville Florida 32611, United States of America*
[3]*Mechanical Engineering, The Pennsylvania State University, University Park, Pennsylvania 16802, United States of America*
[4]*Department of Materials Science and Engineering, University of Florida, Gainesville, Florida 32611, United States of America*
[5]*Department of Chemical Engineering, University of Florida, Gainesville, Florida 32611, United States of America*

There are numerous applications for deep UV AlGaN Light-Emitting Diodes (LEDs) in virus inactivation, air and water purification, sterilization, bioagent detection and UV polymer curing. The long-term stability of these LEDs is also of interest for long-duration space missions such as the Laser Interferometer Space Antenna (LISA), the first gravitational wave detector in space. We review the literature on long-term aging of these devices as a function of drive current, temperature and dc versus pulsed operation. The LEDs typically show a gradual decline in output power (up to 50%) over extended operating times (>100 h) and the rate of decline is mainly driven by current and temperature. Experimentally, the degradation rate is dependent on the cube of drive current density and exponentially on temperature. The main mechanism for this decline appears to be creation/migration of point defects. Pre-screening by considering the ratio of band edge-to-midgap emission and LED ideality factor is effective in identifying populations of devices that show long lifetimes (>10,000 h), defined as output power falling to 70% of the initial value.
 [DOI: 10.1149/2162-8777/acd602]

Manuscript submitted April 21, 2023; revised manuscript received May 12, 2023. Published May 31, 2023. *This paper is part of the JSS Focus Issue on Recent Developments in Theory, Measurements and Applications of Luminescent Materials: A Tribute to Prof. B. Di Bartolo.*

Existing applications for deep UV Light-Emitting Diodes (LEDs) include sterilization, water purification, monitoring nitrates in water, $NO_x$ monitoring emissions from combustion engines, agriculture, light sources for high-density optical memory, short wavelength lithography as well as various curing processes.[1–21] The UV wavelength range is divided into four bands, UVA (315–400 nm), UVB (280–315 nm), UVC (200–280 nm), and vacuum ultraviolet (100–200 nm). UVC radiation is able to inactivate SARS-CoV-2, compromising its viral genome and virion integrity.[13,17] Emission in the UVA region serves as the primary light source in the curing of UV glue,[19] light therapy, air purification,[16,18] and 3D printing.[1,4,8] The UVB and UVC bands correspond to the peaks of the absorption spectra of DNA and RNA, enabling their use in deactivating a range of virus sources.[13,14,16–18] The disinfection capability of these LEDs is used in systems for water purification.[10,11,15,16] UVC sources are also used for medical applications such as purification cycle processing and sterilization. The UVC range from 200–230 nm is safe for human exposure while retaining strong germicidal capabilities.[1,4,8]

These LEDs can be modulated at much higher frequencies than competing UV sources such as Hg or excimer (KrBr or KrCl) lamps and have low noise, flexible form factors and relatively high internal quantum efficiency.[1,8,22–29] An important basic science application will be to provide a discharge capability on the free-flying test masses within the Laser Interferometer Space Antenna (LISA), which will be the first gravitational wave detector in space.[30–32] Since these test masses will be subjected to a constant background flux of galactic cosmic rays and solar energetic particles, which result in a net positive charge on the test masses, a charge management system is needed to minimize the effect of electrostatic forces on gravitational-wave observations. This charge compensation will be achieved by pulsed illumination from arrays of deep UV LEDs.[30–32]

The external quantum efficiency (EQE) of $Al_xGa_{1-x}N$-based UV LEDs decreases rapidly as the molar fraction (x) of Al increases and is typically <0.5 percent for UVC LEDs in the 230–240 nm range [33–40] as shown in Fig. 1.[1] Increasing the Al content generally results in a poor crystallinity of AlGaN epilayers, causing a low internal quantum efficiency (IQE).[41–52] Both *n*-type and *p*-type doping efficiencies of AlGaN are low because of the increase in ionization energies of dopants with increasing Al composition.[1,4,39,40] This leads to high contact resistance and inefficient current injection efficiency into the active region. The light-extraction efficiency of AlGaN UV LEDs grown on *c*-plane sapphire substrates is limited by the valence band structure of high Al content AlGaN, causing a shift in the polarization of light at short wavelength for *c*-plane device structures.[53–60] Emission at germicidal UVC wavelengths is primarily in the transverse electric (TE) polarization mode for a *c*-plane substrate, and thus perpendicular to the substrate surface.[61–66] At shorter wavelengths, the electron-hole recombination causes a change in photon polarization from having the E field perpendicular to the *c*-axis to having the emission being dominated by the transverse magnetic (TM) polarization mode, emitting parallel to the planar surface. This greatly reduces the light extraction from the LED at short wavelengths.[45,67–73] Park et al.[39] and Chu et al.[40] have recently reviewed approaches to improving contact resistance and transparency of the heavily doped contact layers, epitaxial layer quality, light extraction efficiency and current injection efficiency.[34,38,74–96] Despite limitations due to low doping efficiency in the high-Al contact layers on both sides of the junction, electrical efficiencies at a typical 20 mA drive current can exceed 80%.[62,97–114]

It is important to obtain high-quality AlGaN layers to realize high LED efficiencies. Figure 2 shows the internal quantum efficiency for LEDs as a function of dislocation density.[115] It is found that threading dislocations act as non-radiative recombination centers and induce point defects that can create parasitic recombination

*Electrochemical Society Fellow.
[z]E-mail: spear@mse.ufl.edu

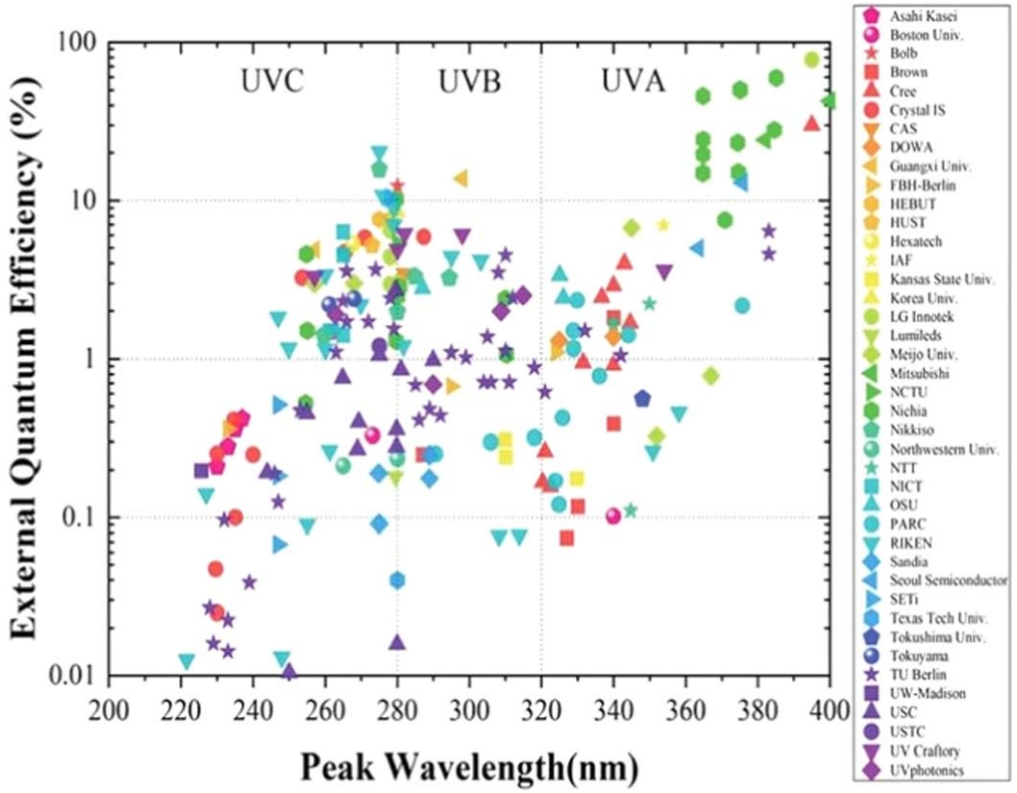


**Figure 1.** Reported EQEs of UV LEDs as a function of emission wavelength. Noticeable is the drop in EQE for wavelengths shorter than 365 nm, which marks the transition from InGaN- to AlGaN-based LED technologies. The full name of abbreviations are: Chinese Academy of Sciences (CAS), Ferdinand-Braun-Institut, Berlin (FBH-Berlin), Hebei University of Technology (HEBUT), Huazhong University of Science and Technology (HUST), Fraunhofer Institute for Applied Solid State Physics (IAF), National Chiao Tung University (NCTU), Nippon Telegraph and Telephone Corporation (NTT), National Institute of Information and Communications Technology (NICT), Ohio State University (OSU), Palo Alto Research Center (PARC), Sensor Electronic Technology, Inc (SETi), Technische Universität Berlin (TU Berlin), University of Wisconsin–Madison (UM-Madison), University of South Carolina (USC), University of Science and Technology of China (USTC). Reprinted with permission from Liang et al.[7] Copyright 2022, John Wiley and Sons.

pathways and compensate intentional dopants.[53,54] As it is difficult to obtain high-quality bulk AlGaN single crystals, it is common to use AlN as a template, to reduce the dislocation density and strain in the LED structure.[62–64,67,69,80,92] Figure 3 shows a deep UV LED structure fabricated on an AlN template grown on a sapphire substrate.[116] This also improves the photon extraction efficiency that is complicated by theTE-to-TM transition. UVC LEDs grown on AlN have higher efficiency at shorter wavelengths than those grown on sapphire substrates, while improving thermal conductivity and minimizing thermal expansion mismatches[5,28,29,39]. Note the complicated layer structure needed to optimize carrier injection and reduce the effects of high resistance on either side of the p-n junction.

Figure 4 shows a deep UV LED structure fabricated on an AlN substrate. Pseudomorphic growth of the LED structure on bulk AlN substrates results in atomically flat epitaxial layers. The reduction in lattice mismatch results in lower strain and reduced threading dislocation density. This reduces non-radiative recombination, point defect densities and three-dimensional growth near the dislocations. A high-resolution Transmission Electron Microscopy (TEM) image of the quantum well region of such a structure is shown in Fig. 5.[3] The lack of dislocations is consistent with pseudomorphic growth on low defect AlN substrates.[34]

The reliability of these light sources is clearly of interest.[62,97–110] Several groups have reported lifetimes over 3500 h at 20 mA, with a logarithmic rate of decline of output power dependent on temperature and drive current.[24,27,46,100,107,111–116] It is common to determine the failure rate at operating temperatures by extrapolating from the failure rate under thermally-accelerated stress conditions through the Arrhenius equation, but this does not capture failure mechanisms that are not accelerated by elevated temperatures.[117–121]

Typical output spectra from such as a structure are shown in Fig. 6, as a function o drive current. The spectrum consists of the main band-to-band emission centered at 237 nm, as well as broad midgap emission peaks around 340 and 470 nm due to defects in the epitaxial layers. The ratio of band edge to midgap emission is an important predictor of LED longevity under operating conditions, since it is a quantitative indicator of how much energy is going into radiative processes compared to processes that promote heating and defect creation and migration.

In this paper we summarize recent progress in quantifying the lifetimes of large populations of deep UV LEDs over a broad range of duty cycles, temperatures and currents. There has been outstanding progress in achieving long lifetimes (many thousands of hours)[57,122–127] by improvements in the quality of the epitaxial layer growth[128–133] and LED fabrication and packaging processes.[7] The lifetimes are still limited by the density of point defects that originate from the initial growth and can also be created and migrate to the active region during subsequent operation. While the main focus is on the deep UVC LEDs, we also discuss some of the literature from UVA LEDs and other wavelengths to place the work in context and take advantage of the large information base on the reliability of those devices.

## Literature Results

There are a significant number of reliability studies in the literature for deep UV LEDs.[41,57,98,122–127,134–146] In general, the results are quite consistent. For example, Glaab et al.[114] reported on the degradation behavior of AlGaN multiple-quantum well (MQW) LEDs emitting at 233 nm. Stressing was performed at a DC current of 100 mA for 1000 h of operation. A strong reduction of the MQW

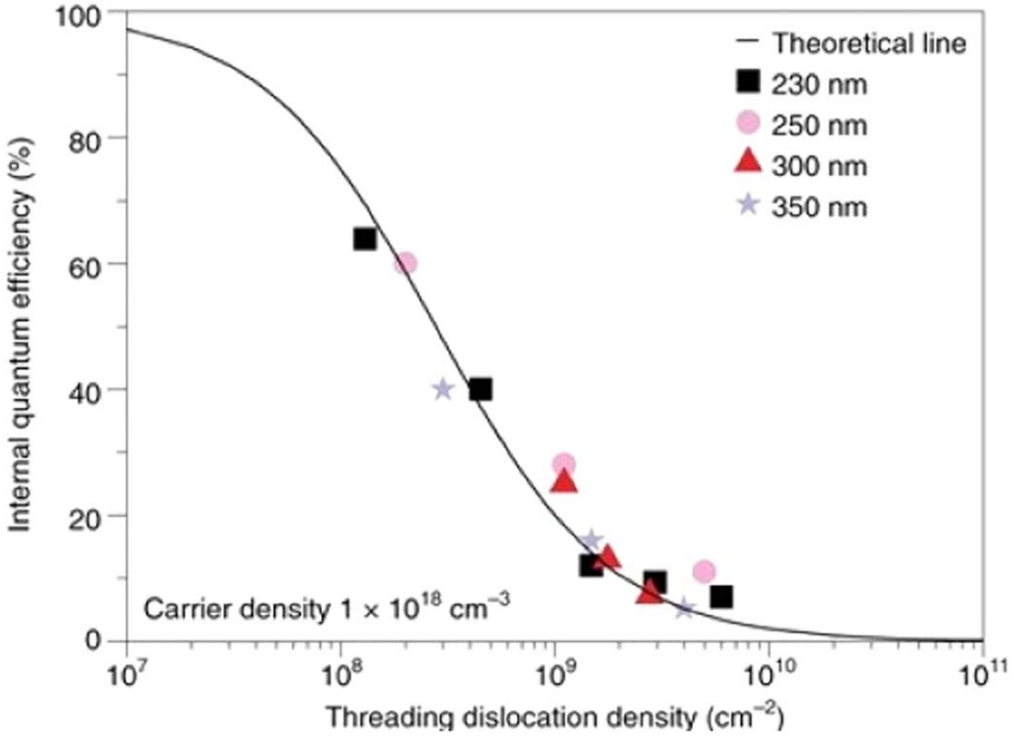


**Figure 2.** IQE of AlGaN MQWs as a function of threading dislocation density for excitation with an excess carrier density of $10^{18}$ $cm^{-3}$. The dislocation density was determined from XRD rocking curves, plan-view TEM and cathodoluminescence. The theoretical calculations are based on a diffusion model of non-radiative carrier recombination at threading dislocations. Figure reproduced from: Ref. 115 with permission The Japan Society of Applied Physics and IOP.

luminescence in the first 250 h and nearly stable MQW emission power over the remaining operation period was observed. Since the band edge emission and that of defect peaks centered at 266 and 403 nm changed with the same trends, this suggested the presence of a common degradation process. During stressing, the leakage current below the turn-on voltage increased. The intensity of another defect peak at 500 nm increased with aging time. The degradation mechanism was suggested to be an increase in the concentration of non-radiative recombination centers in the AlGaN active region.[139–144] The density of point defects acting as centers for trap-assisted radiative recombination outside the active region increased. Typically, the degradation is accelerated by the operation current and temperature[28,40,41,49,57,100,107,126,142–148]

Trivellin et al.[127] summarized mechanisms for the degradation of output power deep UV LEDs during operation and suggested that there were a number of processes that could be present. These included:

i. The creation of non-radiative defects like Ga vacancies along dislocations in the structures, especially related to Mg-doping[101,102,107] that lead to a parasitic leakage path. Cao et al.[103] and Wang et al.[107] suggested that Ga vacancies were induced by loss of substitutional Mg atoms to interstitial sites during LED operation. In other words, the low solubility of Mg on Ga sites in the p-type layers of the LED is a factor in determining reliability. Thus, a key element in optimizing reliability would be to minimize dislocation densities during growth and avoid "over-doping" the p-layers so that loss of Mg from solution is minimized;
ii. Migration of Al atoms from the cladding layers[108,109]
iii. Creation of compensating N vacancies in the p-type electron barrier near the quantum wells,[109] leading to reduced p-type conductivity[110,111]
iv. Migration of donor impurities during LED operation[112]
v. Reactivation of hydrogen passivated Mg acceptors in the p-layers.[113,114] This leads to an initial increase in output power because of the availability of a higher hole concentration
vi. Presence of other defect-impurity complexes such as substitutional carbon on a nitrogen lattice site ($C_N$) and complexes of $C_N$ with oxygen[116,117]
vii. The presence of O impurities in the AlGaN layers produces self-compensation through creation of Al vacancies[149]
viii. Auger recombination during operation creating hot carriers that ionize point defects around the active region, increasing the recombination rate or trap-assisted tunneling conduction[116,118]
ix. Electromigration of contact metals[114] or stress induced by bonding of metals to heat sinks[119]
x. Deterioration of transmittance of encapsulation materials.[120,121] Uedono et al.[122] reported formation of vacancy-oxygen complexes in AlN epitaxial films and suggested these could be a source of grown-in defects in the layers used for the deep UV LEDs. Su et al.[147] reported an increase in concentration of deep trap states at Ec–0.5 eV (E2), 0.68–-0.79 eV (E3), and 0.95–1.2 eV (E4) after current stress.

Kobayashi et al.[148] reported the use of many (20) quantum wells in 226 nm LEDs grown on AlN substrates to improve carrier injection into the active regions and demonstrated lifetimes at 25 °C of >1500 h for 100 mA drive current. They attributed the improved lifetime to the low dislocation density with AlN substrates.[148]

Roccato et al.[149] reported a combined deep level spectroscopy and TCAD simulation study where they identified the traps appearing during aging and then simulated what effect their spatial location would have on the device lifetime kinetics. Three deep trap states at $E_C-0.94$ eV, $E_C-3.06$ eV, and $E_C-3.52$ eV were identified and suggested to be located near the electron blocking layer. The increase of current in the forward-current region below turn-on was suggested to originate from trap-assisted tunneling. The kinetics were also indicative of a diffusion of these trap centers to this location on the p-side of the junction.

Figure 7 summarizes reported degradation mechanisms for deep UV LEDs reported in the literature. Specific to devices grown on AlN substrates, there is 5x improvement in lifetime with a decrease in

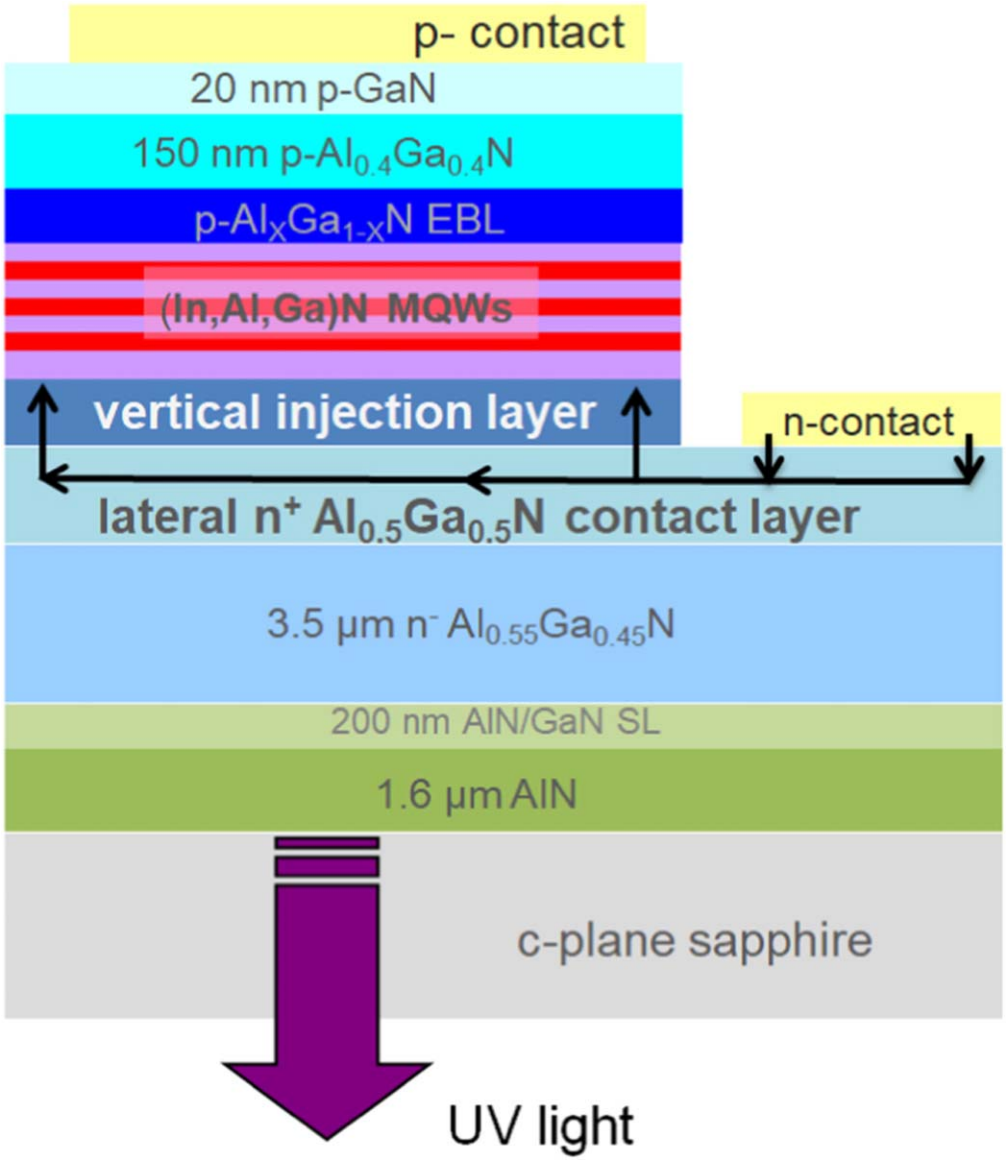


**Figure 3.** Schematic of LED layer structure grown on AlN template on a sapphire substrate. The arrows show the electron flow direction through the lateral n-contact and vertical injection layer to the MQWs.reprinted from Knauer et al.[116], https://doi.org/10.7567/1347-4065/ab0f13, Open access.

oxygen content in the AlGaN layers, as determined by Secondary Ion Mass Spectrometry measurements.[150] It was suggested that oxygen created Al vacancies, but also pointed out that any point defect creation will cause degradation in optical output and hence affect the perceived lifetime. Oxygen impurities in the AlGaN layers produce self-compensation through creation of Al vacancies. Other possibilities for the defects controlling lifetime include the presence of defect-impurity complexes such as substitutional carbon on a nitrogen lattice site ($C_N$) and complexes of $C_N$ with oxygen. We do not believe hydrogen plays a major role, since its main electrical effect is passivation of Mg acceptors and these will reactivate during forward bias operation, producing an increase in emission intensity. The main suspects in terms of impurities are oxygen dn carbon, since these are present from the growth precursors and also native defects such as Ga and Al vacancies.

The literature shows a consistent increase in reverse bias current in the LEDs and an increase in diode ideality factor during long-term operation, as the output power decreases. It is not always the case that midgap defect emission increases, possibly due to trap saturation effects. These observations suggest some approaches to pre-selecting LEDs based on their initial characteristics prior to extended testing, since parametric testing can reveal the presence of a larger than normal population of point defects that can accelerate the degradation. Figure 8 (top) shows a typical set of output power versus time plots for 20 Crystal IS LEDs operated at 20 mA and then for typical devices operated at different drive currents (bottom). The rate of the continuous decay observed depends on drive current and was seen to be correlated to reducing the oxygen content in the epitaxial AlN buffer layer. As was discussed earlier, it was suggested that oxygen in AlN can self-compensate by driving the creation of Al vacancies. The migration of these detects into the active region during LED operation was thought to be one factor producing the loss of output power. It is also worth noting for practical applications that the packaging issue is non-trivial for deep UV LEDs, since the high photon energy can degrade packaging materials. The packaging of DUV-LEDs is challenging due to the following factors:

- High refractive index of packaging materials: The high refractive index of most packaging materials causes significant light reflection and loss, which reduces the light output of DUV-LEDs.
- Chemical instability of packaging materials: Many packaging materials are unstable in the presence of UV radiation, which can lead to degradation of the device performance and reliability.

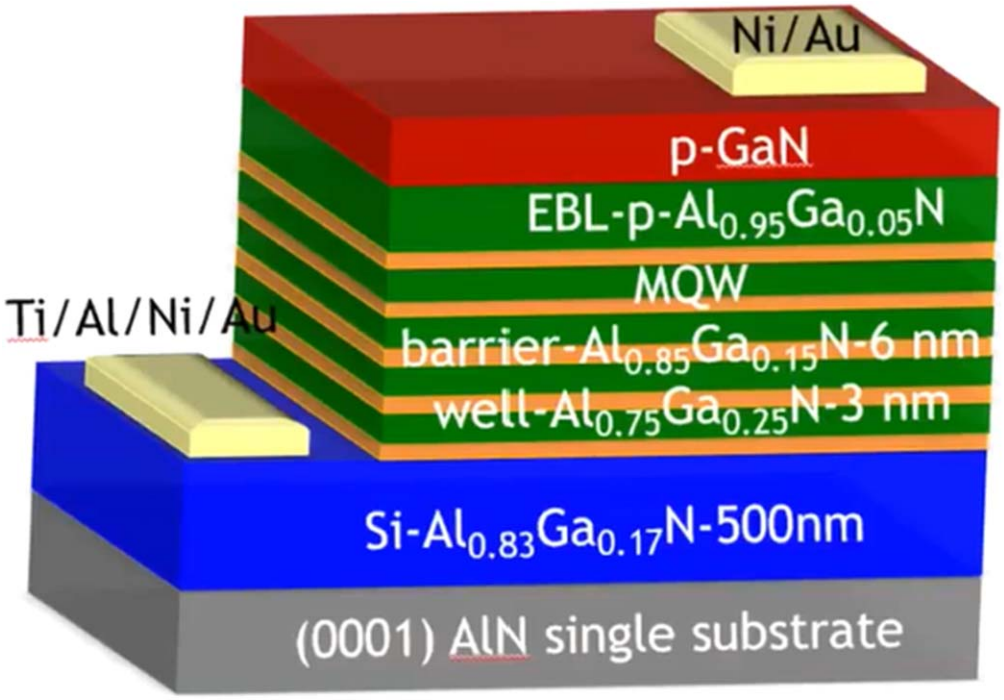


**Figure 4.** Schematic of LED structure grown an AlN substrate. Reproduced from Leo Schowalter, Crystal IS, Pseudomorphic AlGaN Semiconductors: From UVC LED and UVC LD to RF and Power Revolution, IEEE EDS Webinar, Nov 18th, 2020.

- Thermal management: DUV-LEDs generate a significant amount of heat, which must be effectively dissipated to prevent damage to the device.
- Hermeticity: DUV-LEDs must be packaged in a hermetic manner to prevent moisture ingress, which can lead to corrosion and device failure.

A number of different packaging technologies have been developed to address these challenges, including:

- Liquid encapsulation: Liquid encapsulation uses a low-refractive-index liquid to fill the gap between the DUV-LED and the package, which reduces light reflection and loss.
- Hermetic bonding: Hermetic bonding uses a high-temperature, high-pressure process to bond the package to the DUV-LED, which creates a hermetic seal that prevents moisture ingress.
- Active cooling: Active cooling uses fans or heat pipes to actively remove heat from the DUV-LED, which improves the device performance and reliability.

The development of new packaging technologies for DUV-LEDs is an active area of research, and continued progress in this area will be essential for the commercialization of this technology.

What is clear from the literature is

i. Multiple degradation mechanisms may be present[41,108,109,142–150]
ii. Migration of defects already present in the as-grown structure, or created during subsequent operation, can migrate into the active regions.[41,97,142–150]
iii. Careful attention must be paid to removing residual hydrogen incorporated in the epi structure from the growth precursors.[1–4,100,101]
iv. The Mg doping level in the p-layers should not exceed the solid solubility to minimize subsequent loss of Mg from solution and associated creation of Ga vacancies.[107–109]
v. The dislocation density should be minimized, favoring use of AlN substrates and careful optimization of buffer layers.[1–4,149,150]
vi. The purity of the growth precursors and avoidance of oxygen in the growth ambient is critical.[62,149]
vii. The degradation rate is a strong function of current density during operation, showing typically a cube power dependence and also on LED temperature.[41,142–150]
viii. A characteristic of the loss of optical power during extended testing is an associated increase in ideality factor n, due to generation of point defects within or around the active region during the stress and also an increase in the reverse bias leakage current and the subthreshold leakage due to increased defect-assisted carrier tunneling.[1–4]
ix. Pre-selection of LEDs based on parametric testing is desirable.[142]

## Predicting Reliability

There are various approaches to predicting the lifetime of UV LEDs, most of which are based on LEDs of other wavelengths and are not necessarily directly relevant but they do provide guidance. In the early days of compound semiconductor photonic devices, the reliability was generally derived from accelerated stress aging at elevated temperatures.[151] The power output as a function of time, $P_{OUT}$ (t), was then assumed to be given by

$$P_{0UT}\ (t) = P_0 \exp^{-\frac{t}{\tau}}$$

where $P_0$ is the initial power output, t is the time under ageing and $\tau$ is the LED lifetime at a given current, I, and the ratio of lifetimes at different currents is given by $\frac{t}{t_0} = \left(\frac{I}{I_0}\right)^{-n}$ where n is typically found to be between 1.5–2.[151] Degradation mechanisms that were identified from the early days included both those in the semiconductor (point and line defects and their migration during operation), metal contacts (reaction with the semiconductor and metal migration) and those due to bonding and packaging (solder instability, mechanical stress in heat sinks).[147–172]

There have been many studies that have attempted to unravel the complexity created by the presence of multiple degradation or failure modes. As an example, Wang et al.[173] reported a model in which the

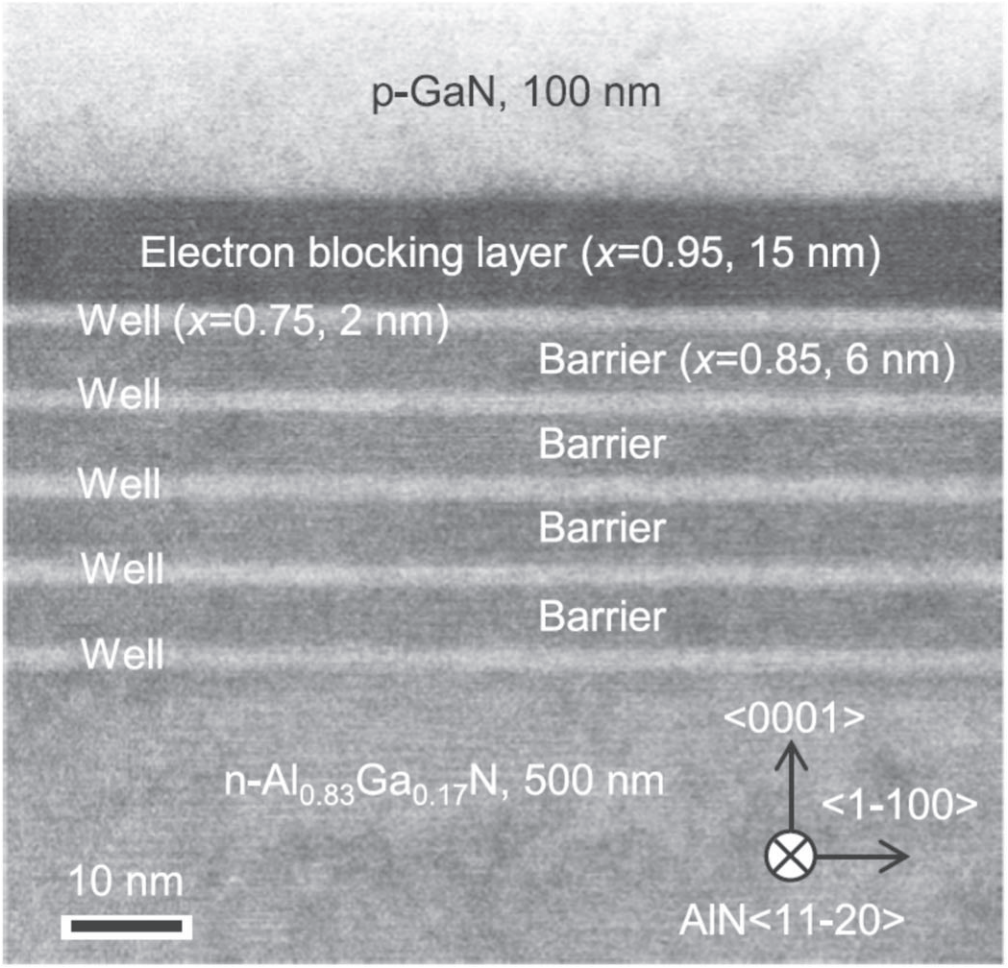


**Figure 5.** Cross-sectional high-angle annular dark field scanning transmission electron microscopy image of UVC LED active region. The LED was grown on a single crystal AlN substrate. Reproduced with permission from Yoshikawa et al., Jpn. J. Appl. Phys.13, 022001 (2020), Copyright Applied Physics Express and IOP.

LED lifetime, $\tau$, was given by

$$\tau = A_{Tj} e^{-\theta T_j}$$

where $A_{Tj}$ and $\Theta$ are constants derived from a weighting of temperature and current-driven stress.

Yang et al.[172] reported an alternative model, developed for white LEDs, which again assumed junction temperature and drive current were the dominant factors, but used multiple-coupled stress ageing rather than constant stress conditions., i.e. different currents at the same temperature and different currents at different temperatures. This dual-stress approach led to a fitted lifetime given by $\tau = I^{-0.17} \exp\left(\frac{4200}{Tj} - 2.58\right)$ and a time dependence for output power as $P_{out} = \beta e^{-\alpha t}$, where $\alpha = CI^n \exp^{-E_a}/kT$. This is a purely empirical relationship and does not include the decay mechanism and thus cannot differentiate between a reduction in light extraction efficiency or internal quantum efficiency. However, it does provide a reasonable fit to experimental data for white LEDs.[172]

Zhang et al.[48] made a quick assessment of the lifetime of transparent UV LEDs employing a p-AlN contact layer LED, through fitting of its EQE-*J* curves before and after short-term reliability test. Their assumption is that after initial burn-in comprising stressing under normal current density for 24 h), LED's EQE usually exhibit an exponential decay with time and then if the observed reduction in efficiency with time is due to defect generation,[48]

$$ECE_{\max} = \gamma Bn^2/An + Bn^2 + Cn^3$$

Where $\gamma$ is the light extraction efficiency, A is the non-radiative recombination rate, B is the radiative recombination rate, C is the Auger recombination rate and n is the injected carrier density. Under conditions where Auger current can be neglected, this leads to a slope of the ECE curve as a function of current density (J) at low injection conditions given by[48]

$$\frac{\delta ECE}{\delta J} = \frac{2LEE.B}{edA^2}$$

Where LEE is the light extraction efficiency, d is the quantum well active region thickness and e is the electronic charge. Under high injection, the corresponding equation is

$$\frac{\delta ECE}{\delta J} = \frac{-ECE}{3J}$$

By fitting the ECE-J curves under different injection levels, this provides a means of extracting the value of $t_a$ as[48]

$$t_a = \frac{B.n}{ECE.\frac{\delta A}{\delta t}}$$

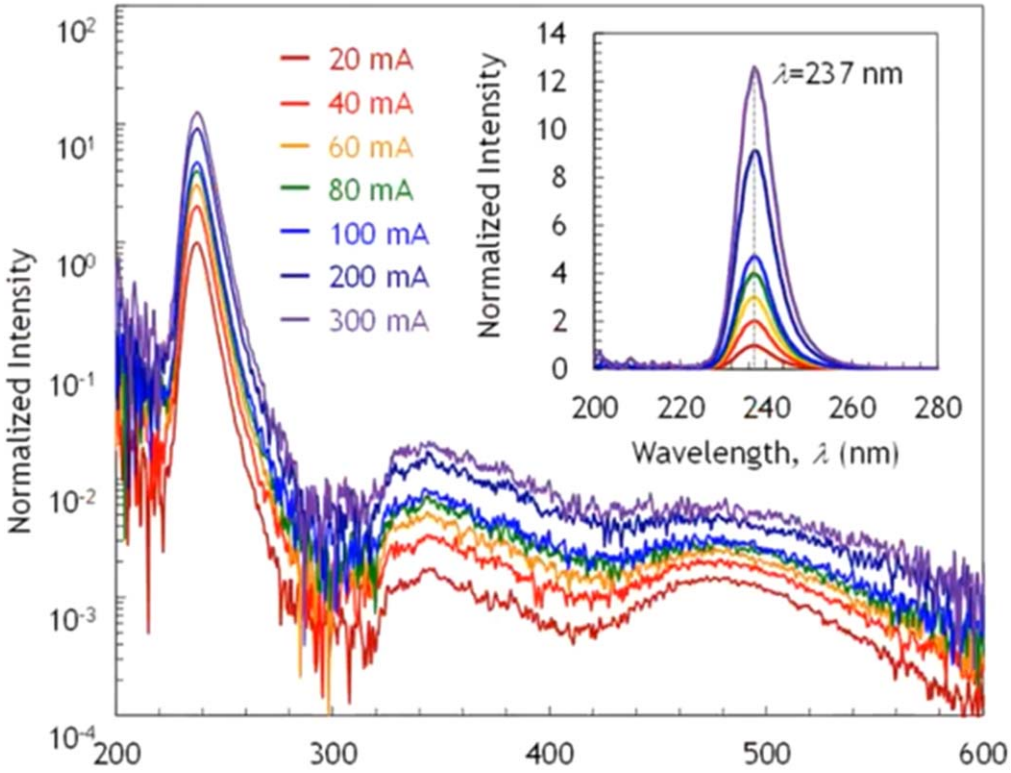


**Figure 6.** Typical emission spectra from UVC LED as a function of drive current.

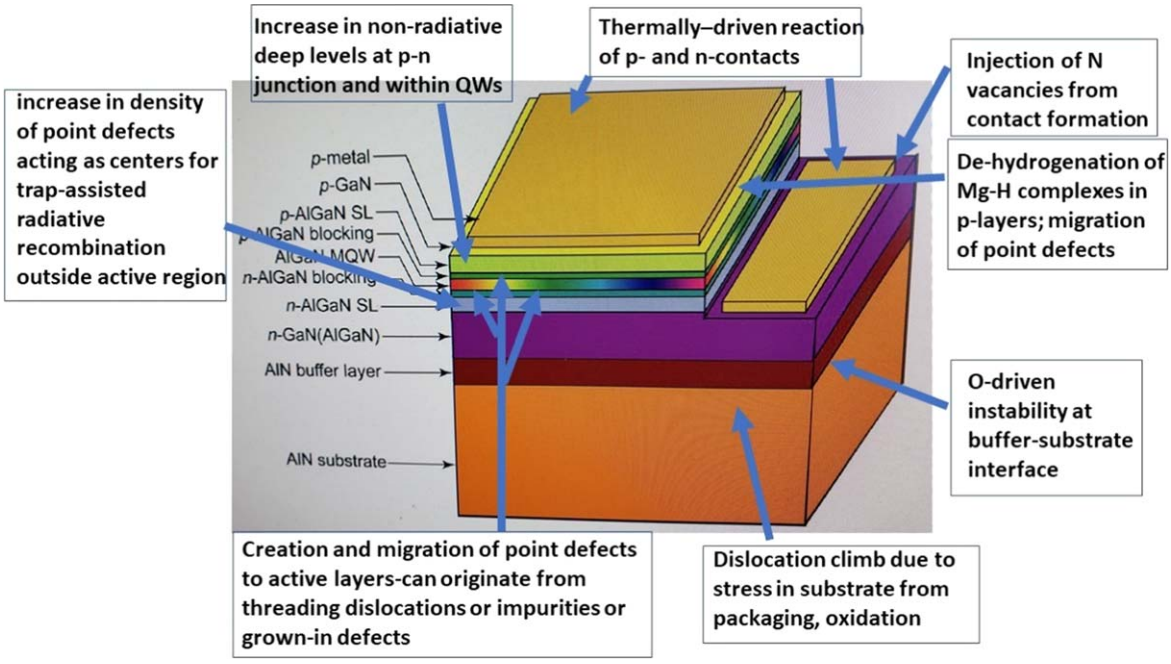


**Figure 7.** Summary of reported degradation mechanisms in UV LEDs. Degradation of output power from UVC LEDs as a function for fixed drive current (a) or a a function of increasing drive current(b). Reproduced from Leo Schowalter, Crystal IS, Pseudomorphic AlGaN Semiconductors: From UVC LED and UVC LD to RF and Power Revolution, IEEE EDS Webinar, Nov 18th, 2020.

In the equation

$$ECE(t) = ECE(0)e^{\frac{t}{ta}}$$

This same group[49] have used this model to extract lifetime data for deep UV LEDs (267–278 nm) as a function of drive current at room temperature and found that larger the current, the bigger the defect maximal multiplication factor and the hotter the junction temperature at a given set of conditions, the bigger the initial defect density in the LED must have been. Typical results are shown in Fig. 9 for two different drive currents and for a premium device in Fig. 10. Note the exceptional room temperature lifetime of over 30,000 h for reduction of output power to 70% of the original value.

Ruschel et al.[122] reported on current-induced degradation and lifetime prediction of LEDs emitting at 310 nm. They found that at long operation times, the degradation rate was almost independent of

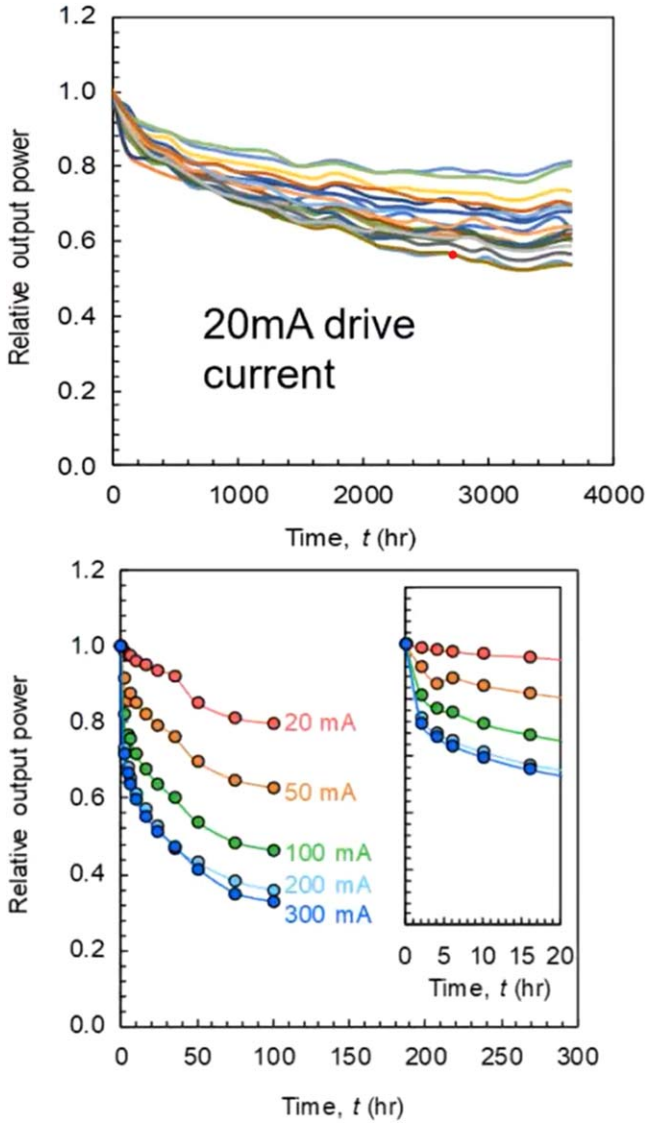


**Figure 8.** Degradation in light output for a population of UVC LEDs as a function of time at fixed drive current (top) and (bottom) the rate of degradation as a function of drive current.

current density, while at short times, this rate was strongly dependent on current density. The mean normalized output power was proportional to the product of aging time and the third power of current density. They fitted their data to the relation[122]

$$t_{70\%} = C_{70\%} J^{-3}$$

where $t_{70\%}$ is the lifetime for a drop of initial output power to the 70% level, J is the current density and $C_{70\%}$ is a constant. The exponent was extracted from the slope of a double logarithmic plot of $t_{70\%}$-J. They also reported that the output power as a function of time, P(t) could be represented as[122]

$$P(t) = -\beta \ln(\alpha J^3 (t + \exp^{-\frac{1}{\beta}})$$

where $\alpha$ and $\beta$ were constants for a given current density. Fits using this equation to their aging data are shown in Fig. 11. The results of Kobayashi et al.[148] were fit to this equation with $\alpha$ of $10^{-6}$ $h^{-1}$ $A^{-3}$ and $\beta$ of 0.053.

Similar fits were reported by Trivellin et al.,[175,176] as shown in Fig. 12 for LEDs with emission wavelengths from 275–280 nm. The commercial devices show a strong correlation between the stress current and the degradation rate and the degradation shows the inverse current dependence suggested by Ruschel et al.[122]

Piva et al.[174] suggested there are two different time regimes for degradation, with the first being over the first ~1000 min of LED operation suggested to be due to de-hydrogenation of Ga vacancies. At this point, there is no direct experimental evidence for this mechanism, although formation of Ga vacancies are energetically favorable in AlGaN. The second time regime at times >1000 min was suggested to be due to generation of midgap traps, with two levels at $E_C-1.6$ and $E_C-2.15$ eV being detected. The initial degradation in optical output is due to a decrease in carrier injection efficiency, while the longer time scale degradation is due to increased carrier recombination.[174]

Zhang et al.[174,176,178] reported a detailed study of radiative recombination of a high internal-quantum-efficiency 268 nm LED within the context of the ABC model.[178–180] They found that while external quantum efficiency was high (~86%), the light extraction efficiency was low (~15%). They also reported long-lifetime UVC LEDs, as already shown in Fig. 10. Their model gives a good fit to the LED lifetime, where the lifetime is proportional to the radiative recombination coefficient and inversely proportional to the product of initial nonradiative recombination coefficient and the rate of growth in defect concentration,[178] whilst also incorporating the known dependence on junction temperature and drive current density.[180,181] The output power is then given by

$$P_t = \frac{A_0 + H}{A_0} \ln(ke^{at} - k + e) + H$$

Where $A_0 = N_{T0}\sigma v$,v is the carrier kinetic energy, $\alpha$ is the defect growth rate, k is a constant, $N_T$ the defect concentration, $H = Bn + Cn^2$ and A is the value of A at zero time. As shown in Fig. 10, the experimental data fits well to the model for $A_0$ in the range $6 \times 10^5$ to $7.6 \times 10^6$ $s^{-1}$, $H = 2 \times 10^7$ $s^{-1}$, k = 3–10 and $\alpha = 5–7 \times 10^{-4}$ $h^{-1}$, with e ranges representing values over a temperature range from 25 °C–60 °C.[182]. At room temperature, lifetime values >10,000 h are possible.as shown in Fig. 10.and assuming a final output power of 80% of the initial value. In that case the fitting parameters were $A_0 = 2 \times 10^6$ $s^{-1}$, $H = 5 \times 10^7$ $s^{-1}$, $k = 10^3$ and $\alpha = 5 \times 10^{-5}$ $h^{-1}$.[183].

The lifetime data indicate that while LED lifetime decreases monotonically with increasing junction temperature and driving current, the functional dependences of these two effects are different. The driving current has a power law effect, whereas junction temperature has an exponential effect.[182–188] Thus the lifetime of LEDs is much more sensitive to the junction temperature than driving current.

It is important to note that most of the models end up with some degree of curve fitting, which reduces the physical insight into the degradation mechanisms.

Specific to the LISA mission application, the LEDs must be capable of operating over a nominal 4-year mission that may be extended to 8 years. The LEDs will operate under a pulsed mode to discharge the metal test masses as they charge due to cosmic rays and solar flares. Given the importance of the scientific mission, the goal was to generate data for at least 2 years to be sure the lifetime trends were consistent with these mission lengths.

### Recent Pulsed vs DC Aging Results

Letson[188–190] recently reported test results from over 200 UV LEDs to characterize both the short-term and long-term performance of these devices over the entire expected operating range of the LISA charge management device. LEDs were tested at 4 temperatures of 20 °C, 40 °C, 60 °C, and 80 °C. At each temperature, devices were tested at either low, medium or high stress driving condition in either a DC or pulsed manner. The devices run in a DC, or continuous, mode were operated at either 1 mA, 20 mA, or 80 mA. The pulsed devices were operated at a driving current of 20 mA and a duty cycle of 5%, or a pulse width of 500 ns. The stress

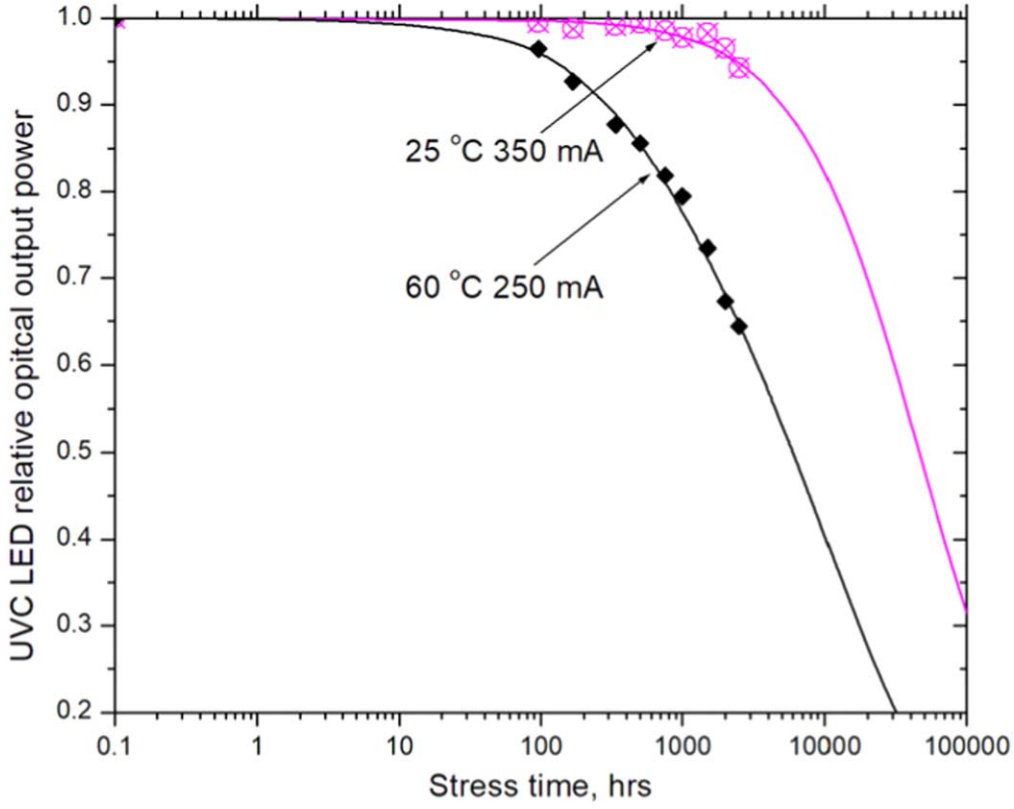


**Figure 9.** Long-term aging characteristics of deep UV LEDs at to different temperatures (a) and lifetime extraction assuming a reduction in output power to 70% of the original value (b). courtesy. Reprinted with permission from Jianping Zhang, Ling Zhou, Ying Gao, Alex Lunev, Shuai Wu, Bolb Inc, Livermore CA, U.S. A.UVC LED Lifetime Models and the defect dynamics under stress (private communication) and PSS (2023).[174]

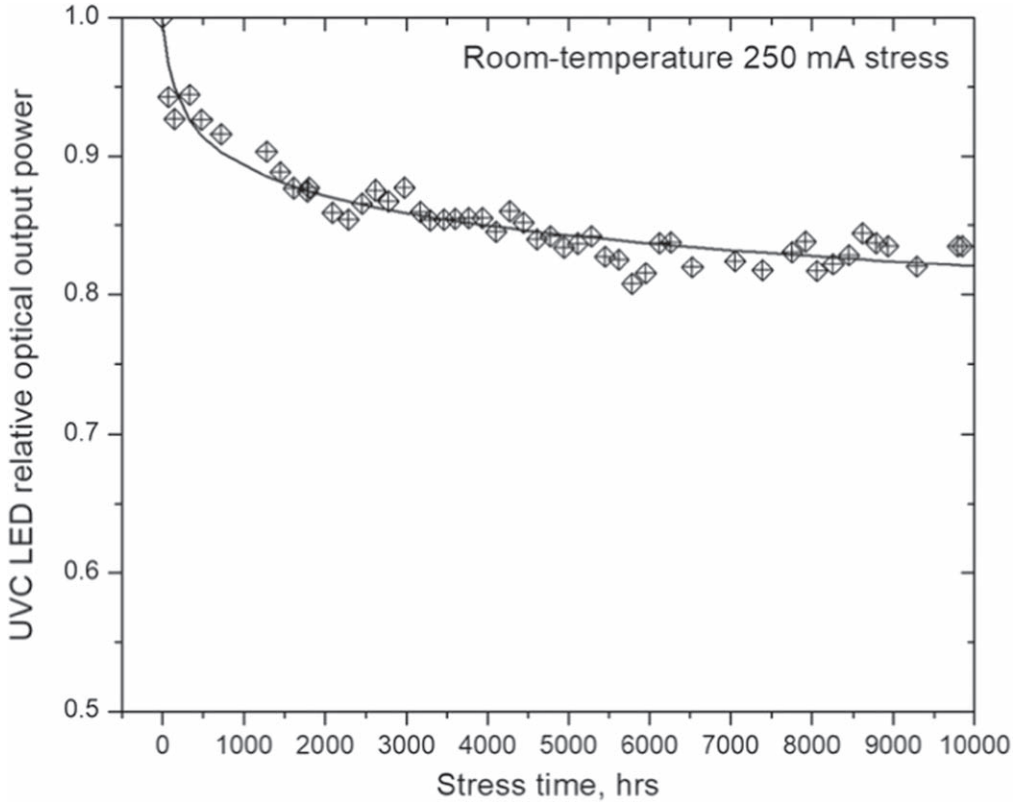


**Figure 10.** lifetime measurement data and fit for a 278 nm UVC LED stressed at 25 °C and 250 mA for 10 000 h. The device maintained an optical output power ≈83.5% of the initial value, reprinted from Ref. 174.

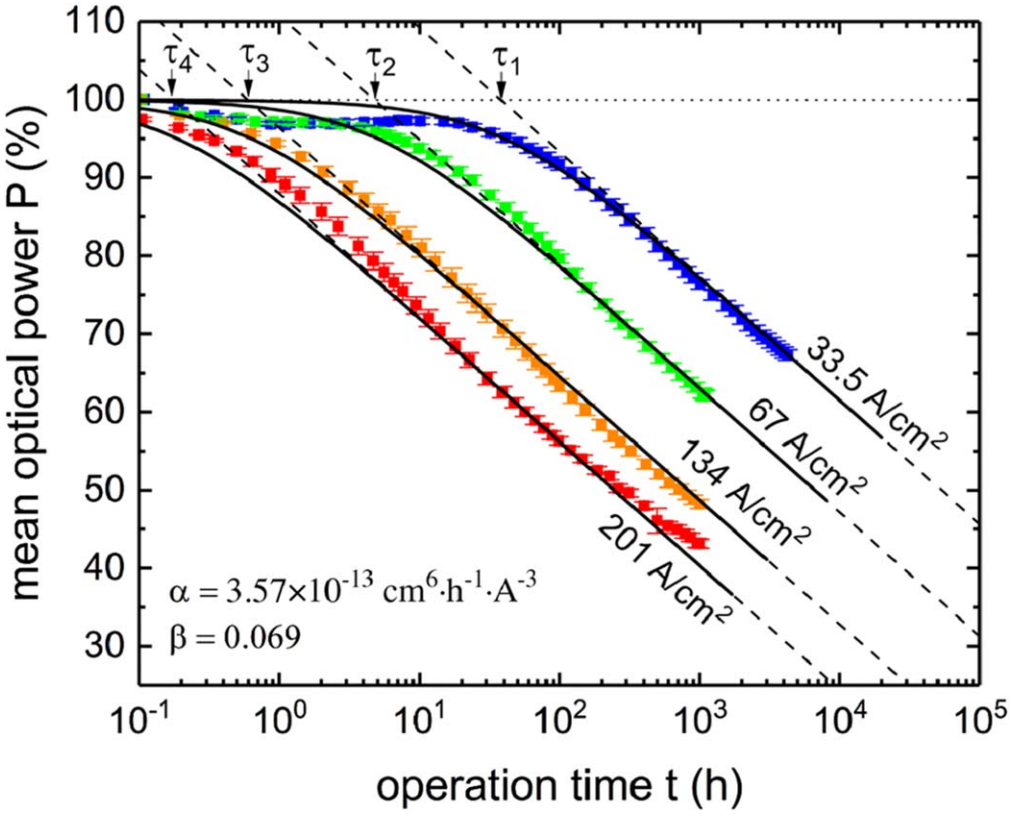


**Figure 11.** Mean normalized optical power versus logarithmic time scale. For different current densities, the characteristic times $\tau\tau$ are indicated. Also shown are the logarithmic functions (dashed lines) and the extended logarithmic function (solid line). Reprinted from Ruschel et al.[123], Open Access.

level was varied for each testing group by limiting the number of cycles of the 100 kHz reference signal in which a UV light pulse was produced. The low stress and medium stress devices only produced a UV pulse in the first 500 cycles and 10,000 cycles of every second, respectively. In contrast, the high-stress case devices pulsed continuously, meaning they produced a pulse in every cycle of the 100 kHz reference signal. In this section, we provide a summary of those results.[188–190] While previous studies of the lifetime of UV LEDs have been done at operating modes relevant for LISA, additional operating modes for the UV LEDs have also since been developed, meaning these new modes will need to be tested on the ground to build confidence that they will be maintainable for the full LISA mission duration.

The parameter survey lifetime test took place over 191 days while 96 UV LEDs were driven in 24 different operating modes while the output power was continuously monitored for each LED. When viewing the power degradation during the lifetime test, it is most intuitive to view the relative power output for each device since the starting power of each LED is different. Thus, by viewing the percent degradation of each LED, comparisons can be made more directly across devices and device types. The data below has been normalized by the power at the beginning of the lifetime test. Specifically, each curve was normalized by the average ADC output between 40,000 seconds and 60,000 seconds from the start of the test. This allows for any temperature-dependent power fluctuations to settle as the rack and LEDs came up to their specified operating temperature. For these tests, we focused on commercial LEDs fabricated on AlN substrates. Figure 13 shows typical I-V characteristics before and after before and after dc aging at 20 °C for 9600 h. The corresponding emission spectra for these devices are shown in Fig. 14. There are only relatively minor changes in these parameters over this 9600 h test.

Since the only metric that matters in terms of LED lifetime for the LISA mission is the ability to produce enough power to effectively discharge the test mass, the driving parameters required to do so don't need to be locked in place. If an LED begins to lose output power over time, the driving parameters can be increased to ensure the device provides enough UV power to discharge the test mass. To make the next lifetime test more representative of flight-like operation, the constant power lifetime tests do just that. Using a closed-loop feedback controller, the lifetime testing software adjust the driving parameters of each LED separately to maintain a constant UV power output over the duration of the test. the previous lifetime test indicated that pulsing the LEDs does not add any extra stress to the device. In fact, the DC continuous mode was more stressful than the pulsed continuous mode. The constant power lifetime test examined the quasi-DC (qDC) continuous mode and the pulsed continuous mode. Continuous discharge power requirements dictate a power level of 0.5 nW in qDC mode, and 2 nW in pulsed mode should be maintained for the mission. To add margin, the qDC and pulsed driving parameters are selected to maintain these target powers with a 2x margin (1 nW qDC and 4 nW pulsed). Only temperatures of 20 °C and 40 °C were used in this lifetime test to avoid activating failure mechanisms in the devices that aren't present at realistic spacecraft temperature.

Figures 15a and 15b show the dc aging data at either 20 or 80 mA and the four different temperatures, while Figs. 15c and 15d show the corresponding pulsed data obtained for either 10, 000 or 100,000 pulses per second at the different temperatures. Current, temperature and pulsed bias repetition rate all influence the degradation of output power. The pulsed data is particularly relevant to a number of applications for deep UV LEDs, since it approximates actual operating conditions.

### Monte-Carlo and Partial Least-Squares Regression

Because there has been little work thus far on correlating indicators of UV LED device quality to their long-term performance, we have recently explored several approaches to use the change in

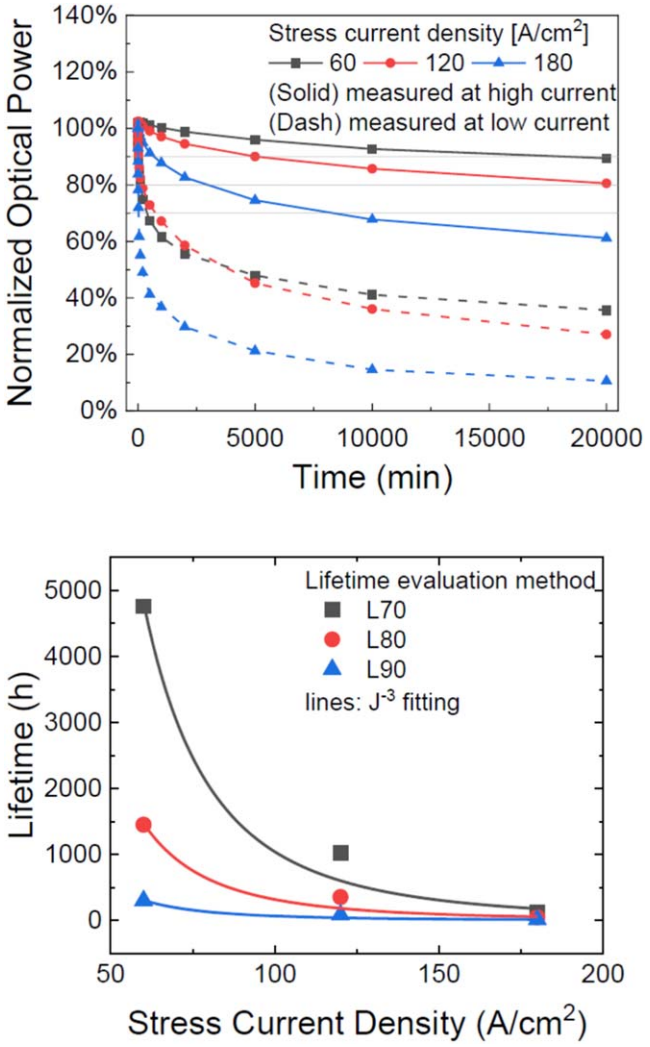


**Figure 12.** (a) Normalized optical power during the degradation at different stress currents (b) Lifetime as a function of stress current density and current inverse cubic fitting. Reprinted from Trivellin et al.[177]

device parameters during aging tests to forecast their reliability. We took 450-day aging data from four different types of tests, quasi-DC testing at either 20 °C or 40 °C and pulsed testing at these same temperatures. Table I shows correlation coefficients for these parameters, but there are none that consistently indicate a strong influence ($\rho > 0.7$) on the long-term performance of these devices in every operating mode. Some of the more promising metrics are the UV ratio, peak height ratio, ideality factor after turn-on, pseudo junction resistance, and 4 V forward current. the metrics considered they are the best. One thing that is interesting to note from the correlation table is that the pre-test metrics seem to have stronger correlations with the performance of the qDC LEDs than the pulsed LEDs. This might be a consequence of the fact the qDC LEDs have consistently degraded more than the pulsed LEDs and it could be true that these pre-test metrics have less influence on the early degradation of the devices and start to influence the performance more as the devices lose more power.

It is also worth mentioning that the correlation is only a measure of a linear dependence between two data sets. Since the physics that governs the performance of these UV LEDs is complex, it is reasonable that there are higher order relationships between these pre-test metrics and the long-term performance that are not obvious in the data. More complex analysis techniques than simple correlations will need to be used in future. Although most of these correlations are weak at best, this information can still be a useful indication of long-term performance.

Even though there are no strong correlations between the pre-test metrics and the lifetime performance, there are some reasonably strong correlations between the pre-test metrics themselves, which violates one of the assumptions of the simplest multiple linear regression techniques. To avoid the issues this typically causes in multiple linear regression problems, a partial least squares regression (PLSR) was used to model a response variable. PLSR works by creating new predictor variables that are linear combinations of the original predictor variables. Each component is created to explain the observed variability in the response variable. The transformed predictor variables of a PLSR model are also orthogonal to one another, so there is zero correlation when ultimately creating the linear model.[174,175] While the goal of a degradation model would be to directly relate the physical properties measured during the lifetime pre-tests, combining the pre-test measurements into components is still a useful practice because the weights of the original predictor variables used to create each component can still be analyzed to determine which metrics the model is placing the most importance on when calculating components that explain the highest variance in the response variable.

***Quality indicators model.***—The first PLSR model approached used the pre-lifetime metrics presented in Table I plus the temperature of the LED and a categorical variable that took a value of 0 for devices operated in the qDC operating mode and a value of 1 for devices operated in the pulsed mode. These last two environmental variables were included in the model so that a single model could be fit to all 96 devices. While future models could look at a more advanced method of accounting for the device temperature and operating condition, simply adding these parameters onto the end of the predictor variables seems to be a reasonable way to account for the device operating conditions. The response variable in this model was the relative integrated current after 450 days of operation. This PLSR model was trained on a randomly selected 50% of the data and the remaining 50% of the device metrics were used as a test set to evaluate the quality of the model. While this model generally predicts the performance of the bulk of the devices well, it struggled to predict the performance of the outlier devices that required more than a 20% increase in integrated current. The higher UV ratios (cleaner spectra) led to less degradation and the presence of a 280 nm parasitic peak increased the device degradation. The only other significant weights in the first 5 components were placed on the ideality factors before and after turn-on. Although the components seem to identify conflicting patterns in the ideality factor before turn-on, the first component (most significant) indicates that higher ideality factors before turn-on lead to reduced power loss while higher ideality factors after turn-on lead to increased power loss. Both results are backed up by the literature in that degradation is caused by the same factors that lead to higher device turn on currents (lower $IF_{off}$) and lower device efficiencies resulting from non-radiative recombination (higher $IF_{on}$). Even though the model did not perfectly predict the performance of these devices, the PLSR model still reflects what is known about the physics of these LEDs and can use this information to predict the long-term performance.

*Spectra and I-V model.*—The other promising PLSR model that attempts to explain the long-term degradation of the continuous LEDs uses a single spectrum and I-V curve to predict performance. Even though the individual data points from a spectrum or I-V measurement may be highly co-linear and contain more than 2000 measurements, the partial least squares algorithm is excellent at reducing the large number of predictor variables into a smaller number of uncorrelated components that can be used to predict the response variable. In this model, the matrix of predictor variables was a 96 × 2112 matrix where each row corresponds to a single sample, or LED, from the lifetime test, and each column corresponds to a measurement at a specific operating condition for all samples. A

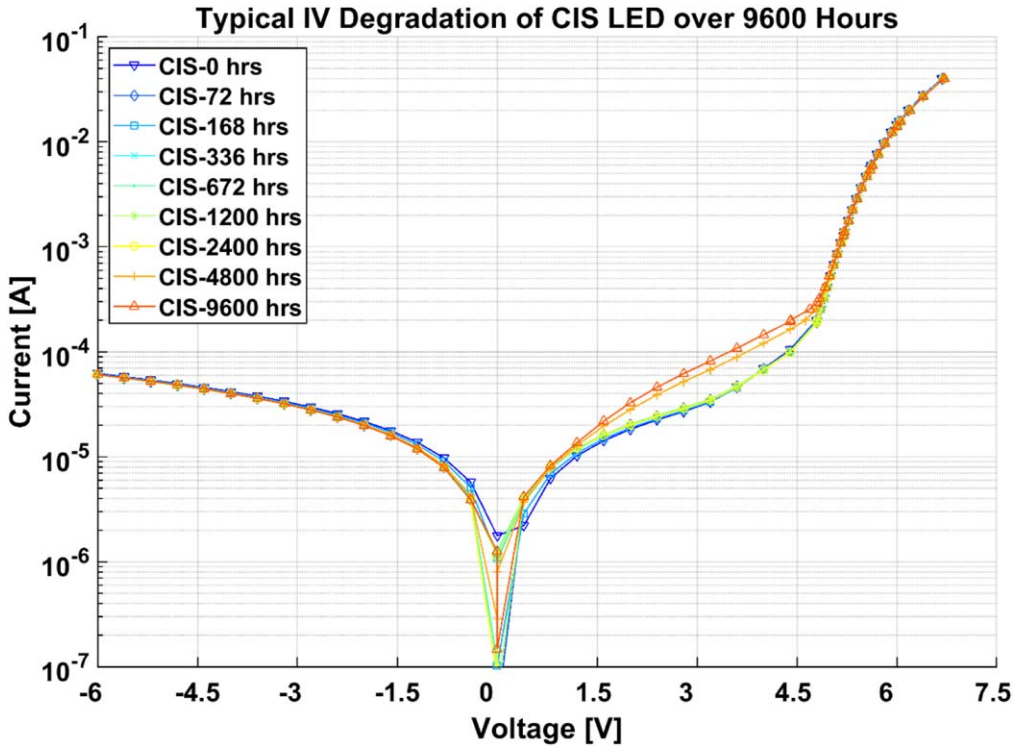


**Figure 13.** I-V Curves for a typical Crystal IS device before and at logarithmic spaced intervals throughout the 400-day lifetime test.

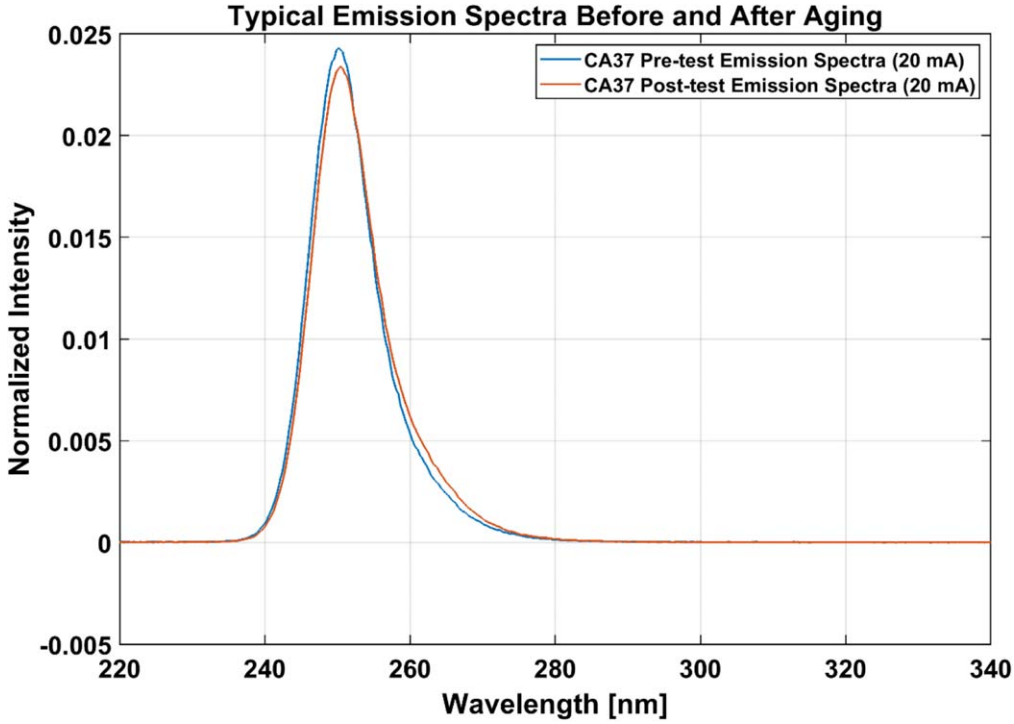


**Figure 14.** Typical emission spectra of a Crystal IS 250 nm device at a constant drive current of 20 mA, before and after 400-days of operation.

single row of the predictor matrix was comprised of the 2047 measurements of spectrum counts taken at 20 mA at uniformly spaced wavelengths between 185.8 nm and 757.7 nm, 63 measurements of the device current taken at uniformly spaced voltages between −6 V and 6.4 V, and then the device operating temperature in °C and a Boolean 0 or 1 corresponding to qDC or pulsed operation.

Since the model uses so many observations to explain a single response variable, care must be taken to not over-fit the model to the training set and create a model that is only useful for predicting results from this set of LEDs. To make sure the model was not over-fit, a randomly selected 20% of the samples were selected as a holdout set that the model was not trained on. With the remaining 80% of data, the PLSR model was trained on a randomly selected

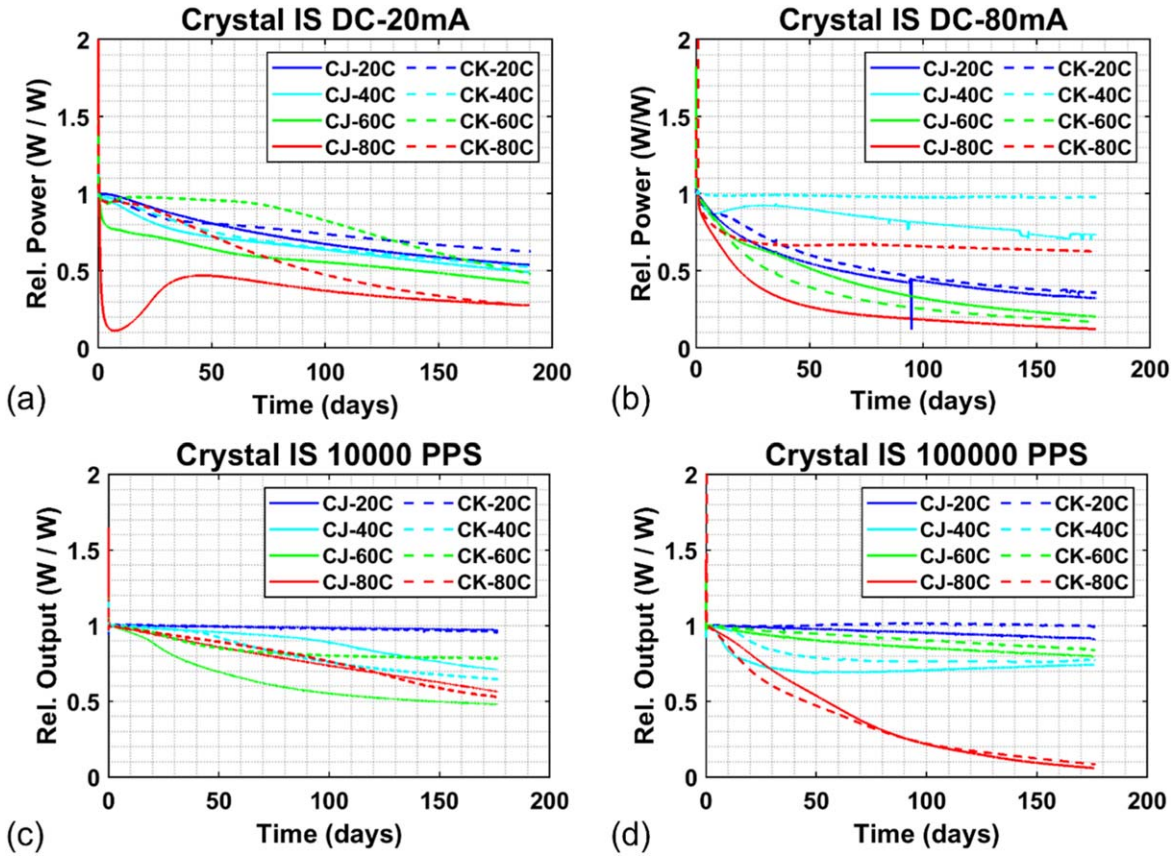


**Figure 15.** Relative power output of 32 Crystal IS 250 nm LEDs at (a) 20 mA constant current for 191 days (b) 80 mA constant current for 177 days (c) 10,000 pulses per second for 177 days and (d) 100,000 pulses per second for 177 days. Each group tested a device from 2 different lots (designated CJ and CK) at temperatures of 20 °C, 40 °C, 60 °C, and 80 °C.

**Table 1. Correlation coefficients between each pre-lifetime metric and the relative increase in integrated current.**

| Metric | qDC-20 °C | qDC-40 °C | Pulsed-20 °C | Pulsed-40 °C |
|---|---|---|---|---|
| UV Ratio | −0.808 | −0.201 | −0.156 | 0.015 |
| Low Power | −0.123 | −0.364 | 0.290 | 0.342 |
| High Power | −0.062 | −0.362 | 0.321 | 0.0112 |
| Parasitic 280 | −0.162 | 0.516 | 0.109 | 0.289 |
| Peak Height ratio | 0.480 | 0.192 | 0.005 | −0.091 |
| $IF_{off}$ | −0.270 | −0.167 | −0.205 | 0.044 |
| $IF_{on}$ | 0.553 | 0.222 | 0.319 | −0.217 |
| Leakage | −0.501 | 0.185 | −0.051 | 0.094 |
| Current Pseudo | −0.344 | −0.303 | −0.101 | 0.240 |
| Junction resistance at 4 V Current | 0.366 | 0.267 | 0.235 | −0.035 |
| Turn-on | 0.443 | 0.014 | 0.242 | 0.089 |
| 6 V current | −0.236 | 0.285 | −0.349 | 0.088 |

50% of the data and the model parameters were saved. After 20 iterations of this process, the average model parameters were used in the final.

PLSR model to evaluate the expected relative IC value for both the training and test sets. The resulting evaluation of the spectrum and IV PLSR model is shown in Fig. 16. This model predicts the relative IC after 450 days more precisely than the quality indicator model and is also able to predict the large degradation seen in the outliers more accurately than any other model.

Several other PLSR models were considered, including those that just used a spectrum measurement or an I-V curve of the device, but using both the spectrum and IV measurements of a single device gave the PLSR model higher predictive power for the devices that had degraded more than average. The PLSR model was determined using only 15 components since this was enough to explain 98.9% of the variance in the response variable. For the spectral contributions, the PLSR model correctly places positive weights on the mid-gap emission peak centered around 475 nm indicating that a more prevalent parasitic peak indicates the device will degrade more in the long term. Interestingly, the top 8 components indicate that different wavelengths of the main peak have different influences on the reliability. In the first two components, the low wavelength peak centered around 252 nm increases the predicted degradation while the second peak centered around 258.7 nm decreases the predicted degradation. Later components tell conflicting stories of the contribution of the main spectrum peak; however the contribution of the main peak has a similar magnitude as each contribution attributed to the mid-gap emission peak. Since the LEDs typically don't have

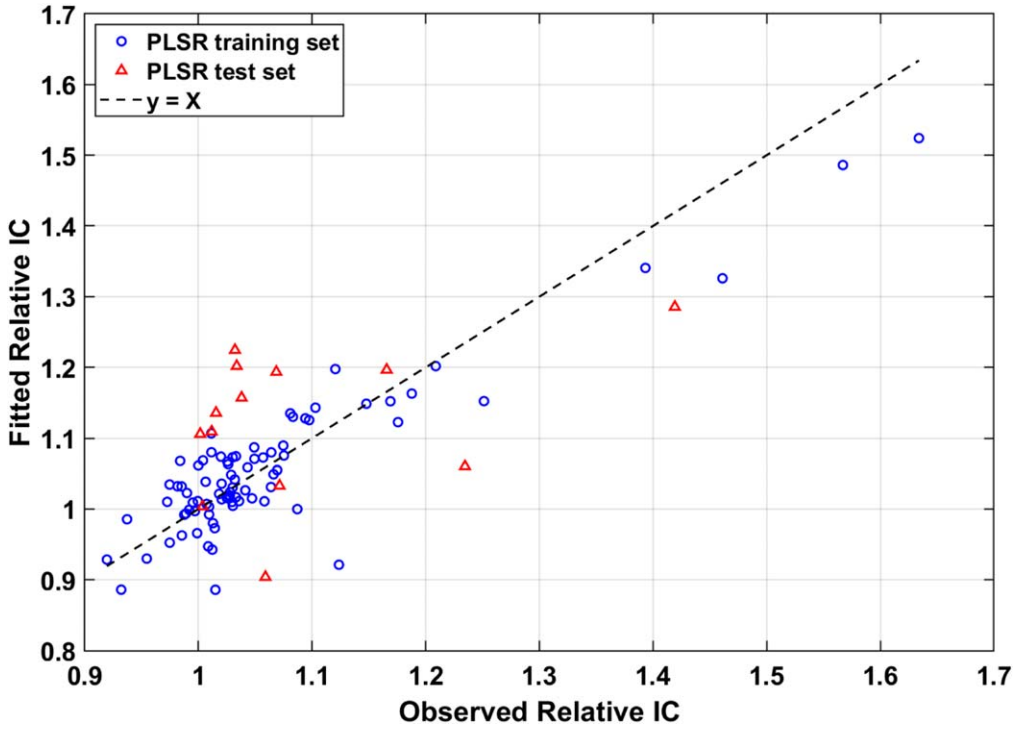


**Figure 16.** Spectrum and IV PLSR model evaluation on the training and test data sets.

differences in the peak wavelength or FWHM of the main peak, this region of the component weights is more difficult to interpret than other regions of the model weights. The I-V influence weight plots are shown on a log-y scale so the contribution of each voltage can be seen. These subplots show the absolute value of the model weights, however negative weights are indicated by a red dot. Although these contribution plots are difficult to interpret, the main takeaways from the I-V contribution plots are firstly that all components place much more significant weights on the region of the I-V curve above 5 V. Secondly, the majority of the eight components place a negative weight on some portion of the reverse bias region of the I-V curve. Since the current produced in this region is negative, the product of the current and negative weight leads to a higher predicted integrated current, or more degradation, which is also predicted by the device physics. The first two components place a positive weight on the majority of the I-V curve after turn-on. A higher current draw at a constant voltage would generally indicate a more efficient LED, however it seems that after turn-on, the I-V curves value a lower current draw. The last 5 components however place a negative weight on most or all the I-V curve after turn-on, meaning a more efficient device should indicate a higher long-term reliability as expected from the model. Finally, the model places a positive weight on the operating temperature, indicating hotter devices degrade faster. The most significant contributions also place a negative weight to the operating condition of the device, indicating devices run in the pulsed mode typically degrade less than the qDC devices. Although the higher order components have varying signs assigned to the operating condition, the weights with greatest magnitude all validate the data.

*Monte Carlo lifetime projections.*—Since one of the applications for UV LEDs is in the charge management system of the LISA space mission, it is of interest to project the degradation of the LEDs to get an idea of how a single LED would perform over the entire LISA mission. In a worst-case degradation scenario (ignoring infant mortality or catastrophic failure or the device), the integrated current would increase exponentially with time. As a device required a higher integrated current to meet discharge power requirements, the integrated current would begin to increase the degradation rate of the device and the degradation would accelerate with time in a type of positive feedback loop. As previously mentioned, however, the integrated current appears to increase linearly with time after an initial nonlinear period. While this exponential increase in IC does not exactly fit all the data that has been collected thus far, it is still beneficial to look at this worst-case scenario to project the degradation of the devices several years into the future.

As with the parameter survey lifetime tests, a Monte Carlo simulation was performed on the data from each case to get an estimate of the integrated current at several points in the future. To generate the 10,000 samples needed for the Monte Carlo analysis, first a two-term exponential equation was fit to each relative IC time series. An example of the Monte Carlo projection for the pulsed discharge mode at 20 °C is seen in Fig. 17, which shows the 8-year exponential projections of the simulated devices in blue, and the data from the 24 real devices being tested at that operating mode overlaid in red. Similar plots were generated for dc and pulsed testing at different temperatures. The 95th and 99th relative integrated percentiles after eight years are indicated by the black dashed lines in the projection plot. A histogram of the relative integrated currents after 8 years can be seen to the right of the projection plot which gives a better picture of the IC distribution for each group. The relative IC percentiles are also tabulated in Table II for each operating case. LEDs in the qDC operating mode can be driven up to a relative IC of 1000 before they reach DC operation of 20 mA and LEDs being operated in the pulsed mode can be driven up to a relative IC of 50 before they reach 100,000 pulses per second, 10% duty cycle, and 20 mA. At these points for both driving cases, the drive current can be increased up to 80 mA, however this would accelerate the degradation.

The results of the Monte Carlo simulation show that even after 8 years of continuous operation, the test data predicts with 99% confidence that the pulsed case LEDs will require an integrated current twice as high as at the start of the mission which is nowhere near the maximum operation of these LEDs. Similarly, 99% of the 20 °C qDC LEDs should require an integrated current 4.79 times higher than at the start of this mission, which represents a qDC duty

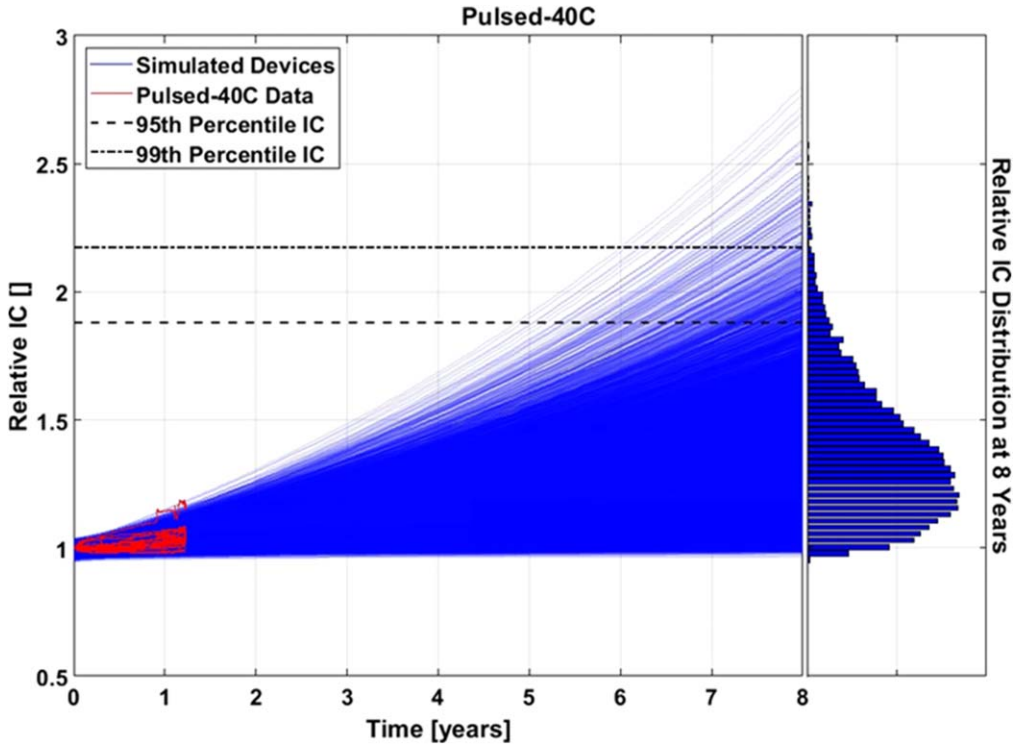


**Figure 17.** Monte Carlo simulation of the relative IC growth of 10,000 devices operated in the pulsed discharge mode at 20 °C. A histogram of relative ICs after 8 years is included at right.

**Table 2. Relative integrated current percentiles after 8 years of continuous discharge.**

| Operating Mode | 95th Percentile | 99th Percentile |
|---|---|---|
| qDC-20 °C | 3.30 | 4.65 |
| qDC-40 °C | 19.23 | 39.05 |
| Pulsed-20 °C | 1.52 | 1.82 |
| Pulsed-40C °C | 1.88 | 2.12 |

cycle of only 0.48% if we consider the operating mode used in this lifetime test. For the qDC 40 °C devices, the Monte Carlo simulation predicts that after 8 years, 99% of the devices will require an integrated current ≈40 times higher than at the start of the test, but even this relatively high integrated current still only represents a qDC duty cycle of 4%, well below DC operation of the UV LEDs. Since the projected integrated current required from each of these four cases is still so far away from driving these devices anywhere near DC or continuous pulsed mode, it seems the assumption to ignore sudden failures or rapid increases in current resulting from driving these devices in a way that would be considered a high stress is valid.

**Table 3. Relative Integrated Current Percentiles after 8 years of continuous discharge when considering only the best 50% of tested devices according to the pre-lifetime rankings.**

| Operating Mode | 95th Percentile | 99th Percentile |
|---|---|---|
| qDC-20 °C | 1.40 | 1.51 |
| qDC-40 °C | 3.66 | 4.75 |
| Pulsed-20 °C | 1.75 | 2.06 |
| Pulsed-40 °C | 2.05 | 2.41 |

*LED screening.*—While the results of the Monte Carlo simulation are immediately very promising, it is important to emphasize that the devices being used in this lifetime test were selected in such a way that the variability in device quality was maximized to get a sufficient spread of pre-test parameters to correlate to lifetime performance. These device parameters have been discussed in detail already, but as an attempt to simulate a realistic flight scenario where only the "best" devices are selected for use in the flight hardware, the Monte Carlo simulation was rerun using only the top 50% of devices in each group, according to the pre-test rankings that were used to sort the devices before the lifetime test.

The rank screened Monte Carlo simulation shows that when only the best 12 devices from each group in terms of UV power, spectral ratio, and electrical characteristics are used to generate statistics for a simulated population of LEDs, the 99th percentile of relative integrated current after 8 years is greatly reduced for both of the qDC cases. The LEDs ranked in the bottom 50% of their group included the single device from the 20 °C group which experienced a sudden failure after 225 days, and all five devices from the 40 °C group whose integrated current had increased by more than 25% since the start of the test. Since the LEDs in the two pulsed groups hadn't degraded by very much in the first 450 days, eliminating the worst 50% of devices had a very small effect on these cases. It is possible that in this pulsed mode, the LEDs haven't been operating for long enough to see any meaningful separation of the LEDs yet so while eliminating the worst devices from these groups has little effect when looking at the first 450 days of data, it is still very possible that over longer time scales, the lower ranked devices would begin to show a more distinct separation from the devices that were higher ranked.

The two lifetime tests that have been run thus far clearly show these state-of-the-art UVC LEDs suffer from high device-to-device variability which can affect their long-term performance. Even though both tests have provided a very high level of confidence that both the continuous and intermittent discharge modes needed for LISA will be successful, simple screening methods have been able to

show that we have enough of an understanding of these devices to use simple pre-screening tests to select devices that will improve the long-term performance of the LISA flight hardware.

## Summary and Conclusions

The light output power, external quantum efficiency, operation voltage, and long-term stability of UVC LEDs with wavelengths from 280 nm down to 200 nm is still not at the level of maturity of visible LEDs. Critical challenges include low resistance UV-reflective contacts as well as efficient carrier injection which can be addressed by novel approaches like tunnel-junctions and polarization doping. Techniques such as laser liftoff coupled with backside shaping for enhanced light extraction are more difficult to incorporate in UVB/C LEDs with high-Al composition AlGaN layers. Some initial reports of n- and p-type doping of AlN also open exciting possibilities for devices with emission wavelengths down to 210 nm. Devices emitting near 230 nm with output powers >3 mW. The efficiency is still low due to changes in the polarization of light emission, high concentrations of point defects as well as carrier injection in AlGaN MQWs, which are partially mitigated by optimized growth on bulk AlN substrates. The devices show a characteristic reduction in optical output over hundreds or thousands of hours, with the rate of decline dependent on drive current, duty cycle and temperature. Much of the degradation appears due to point defect creation during device operation perhaps involving recombination-enhanced reactions. Over-doping the p-layers also leads to performance and reliability issues due to Mg interstitial formation and interactions residual hydrogen.[191,192] This means it is important to use methods to pre-select devices that begin with low concentrations of grown-in defects and two parameters to use in this selection are the ideality factor and ratio of band-edge to midgap emission. The stability of the AlN/AlGaN interfaces at high Al content are also important and require a low background concentration of oxygen within the layers.

The role of hydrogen is still unclear. Since it can passivate Mg acceptors and is present from the precursors in MOCVD growth environment, it can affect the output power of the LED. However, as the device is operated, the injection of electrons can de-passivate the acceptors, leading to a high hole concentration and an increase in emission intensity. This mechanism has been identified previously in heterojunction bipolar transistors where the carbon base dopants reactivate during device operation[193]. The kinetics of this process are usually too fast to be noticeable under DC operation, but we have observed such increases in the pulsed operation data.

Recent lifetime tests leveraging pre-test screening using parametric selection based on ideality factor and bandedge-to-midgap emission have been used to create a model that can predict the long-term performance of these devices. A partial least squares regression technique was used to create two different models; one that uses the pre-test quality indicators, and one that uses the pre-test spectrum and current-voltage measurements. Both models show an agreement with the physics-based interpretations of the test results and validate that there is an important relationship between the fabrication quality of the LEDs and their long-term performance.

State-of-the-art deep UV LED technology is ready to replace Mercury-vapor lamps as the UV light source for contactless discharge in space. Although the commercial technology is relatively new, the devices are already at a state that will allow them to meet all the LISA mission's performance and lifetime requirements.[194,195]

## Acknowledgments

This work was supported by the NASA Earth Science Technology Office (ESTO) grant 80NSSC20K0324. The authors wish to thank Dr Jerry Zhang, Bolb, Inc. for sharing his data prior to publication. The work at UF was also performed as part of Interaction of Ionizing Radiation with Matter University Research Alliance (IIRM-URA), sponsored by the Department of the Defense, Defense Threat Reduction Agency under award HDTRA1–20–2–0002. The content of the information does not necessarily reflect the position or the policy of the federal government, and no official endorsement should be inferred. AH also acknowledges support from the US National Science Foundation (ECCS # 2015795). The work at UF was also supported by NSF DMR 1856662.

## ORCID

Stephen J. Pearton https://orcid.org/0000-0001-6498-1256

## References

1. M. Kneissl, T. Y. Seong, J. Han, and H. Amano, *Nat. Photonics*, **13**, 233 (2019).
2. M. S. Shur and R. Gaska, *IEEE Trans Electron Dev.*, **57**, 12 (2010).
3. A. Yoshikawa, R. Hasegawa, T. Morishita, K. Nagas, and S. Yamada, *Appl. Phys. Express*, **13**, 022001 (2020).
4. Y. Chen, J. Ben, F. Xu, J. Li, Y. Chen, X. Sun, and D. Li, *Fundamental Research*, **1**, 717 (2021).
5. J. R. Grandusky, S. R. Gibb, M. C. Mendrick, C. Moe, M. Wraback, and L. J. Schowalter, *Appl. Phys. Express*, **53**, 082101 (2011).
6. Y. Nagasawa and A. Hirano, *Photonics Res.*, **7**, B55 (2019).
7. S. Liang and W. Sun, *Adv. Mater. Technol.*, **7**, 2101502 (2022).
8. R. Choi, *Proc. SPIE*, **10104**, 101041N (2017).
9. P. J. Parbrook and T. Wang, *IEEE J. Sel Topics Quantum Electron*, **17**, 1402 (2011).
10. M. Wurtele, T. Kolbe, M. Lipsz, A. K¨Ulberg, M. Weyers, M. Kneissl, and M. Jekel, *Water Res.*, **45**, 1481 (2011).
11. K. A. Sholtes, K. Lowe, G. W. Walters, M. D. Sobsey, K. G. Linden, and L. M. Casanova, *Environ. Technol.*, **2016**37, 2183 (2016).
12. P. O. Nyangaresi, Y. Qin, G. Chen, B. Zhang, Y. Lu, and L. Shen, *Water Res.*, **157**, 218 (2019).
13. H. Inagaki, A. Saito, H. Sugiyama, T. Okabayashi, and S. Fujimoto, *Emerging Microbes and Infections*, **9**, 1744 (2020).
14. J. Glaab et al., *Scientific Rep.*, **11**, 14647 (2021).
15. T. Matsumoto, I. Tatsuno, and T. Hasegawa, *Water*, **11**, 968 (2019).
16. K. Sholtes and K. G. Linden, *Water Res.*, **165**, 114965 (2019).
17. S. Liu et al., *Adv. Funct. Mater.*, **31**, 2008452 (2021).
18. H. Zhang, X. Jin, S. S. Nunayon, and A. C. Lai, *Indoor Air*, **30**, 500 (2020).
19. A. Endruweit, M. Johnson, and A. Long, *Polym. Compos.*, **27**, 119 (2006).
20. M. Schreiner, J. Martínez-Abaigar, M. Glaab, and M. Jansen, *Optik Photonik*, **9**, 34 (2014).
21. P. E. Hockberger, *Photochem. Photobiol.*, **76**, 561 (2002).
22. J. Han, M. H. Crawford, R. J. Shul, J. J. Figiel, M. Banas, L. Zhang, Y. K. Song, H. Zhou, and A. V. Nurmikko, *Appl. Phys. Lett.*, **73**, 1688 (1998).
23. M. Kneissl and J. Rass, *J. III-Nitride Ultraviolet Emitters* (Springer, Berlin/Heidelberg, Germany) (2016).
24. Y. Nagasawa and A. Hirano, *Appl. Sci.*, **8**, 1264 (2018).
25. M. Guttmann, F. Mehnke, B. Belde, F. Wolf, C. Reich, L. Sulmoni, T. Wernicke, and M. Kneissl, *Jpn. J.Appl. Phys.*, **58**, SCCB20 (2019).
26. D. Liu et al., *Appl. Phys. Lett.*, **113**, 011111 (2018).
27. H. Hirayama, "Recent progress in AlGaN Deep-UV LEDs." *Light-Emitting Diode An Outlook On the Empirical Features and Its Recent Technological Advancements*, ed. J. Thirumalai (IntechOpen, London) (2018).
28. C. G. Moe, S. Sugiyama, J. Kasai, J. R. Grandusky, and L. J. Schowalter, *Phys. Status Solidi A*, **215**, 1700660 (2018).
29. J. R. Grandusky, J. Chen, S. R. Gibb, M. C. Mendrick, C. G. Moe, L. E. Rodak, G. A. Garrett, M. Wraback, and L. J. Schowalter, *Appl. Phys. Express*, **6**, 032101 (2013).
30. D. Hollington, J. T. Baird, T. J. Sumner, and P. J. Wass, *Class. Quantum Grav.*, **2**, 1 (2015).
31. P. J. Wass, H. M. Araújo, D. N. Shaul, and T. J. Sumner, *Class. Quantum Grav.*, **22**, S311 (2005).
32. P. Wass, "LISA pathfinder collaboration, free-fall performance for the LISA gravitational wave observatory." *New results from LISA Pathfinder APS April Meeting Abstracts*, **2018**, C14 (2018).
33. M. Shatalov, W. Sun, A. Lunev, X. Hu, Y. B. Alex Dobrinsky, J. Yang, M. Shur, C. G. Moe, M. Wraback, and R. Gaska, *Appl. Phys. Express*, **5**, 082101 (2012).
34. J. R. Grandusky, J. A. Smart, M. C. Mendrick, L. J. Schowalter, K. X. Chen, and E. F. Schubert, *J. Cryst. Growth*, **311**, 2864 (2009).
35. J. R. Grandusky, S. R. Gibb, M. C. Mendrick, C. G. Moe, M. Wraback, and L. J. Schowalter, *Appl. Phys. Express*, **4**, 082101 (2011).
36. C. G. Moe, J. R. Grandusky, J. Chen, K. Kitamura, M. C. Mendrick, M. Jamil, M. Toita, S. R. Gibb, and L. J. Schowalter, *Proc. SPIE*, **8986**, 89861V (2014).
37. C. Chu, K. Tian, J. Che, H. Shao, J. Kou, Y. Zhang, Y. Li, M. Y. Wang, M. Y. Zhu, and Z. H. Zhang, *Opt. Express*, **27**, A620 (2019).
38. F. Mehnke, T. Wernicke, H. Pingel, C. Kuhn, C. Reich, V. Kueller, A. Knauer, M. Lapeyrade, M. Weyers, and M. Kneissl, *Appl. Phys. Lett.*, **103**, 212109 (2013).
39. J.-S. Park, J. K. Kim, J. Cho, and T.-Y. Seong, *ECS J. Solid State Sci. Technol.*, **6**, Q42 (2017).
40. C. Chu, K. Tian, Y. Zhang, W. Bi, and Z.-H. Zhang, *Phys. Status Solidi A*, **216**, 1800815 (2019).

41. T. Kinoshita, T. Obata, T. Nagashima, H. Yanagi, B. Moody, S. Mita, S.-ichiro Inoue, Y. Kumagai, A. Koukitu, and Z. Sitar, *Appl. Phys. Express*, **6**, 092103 (2013).
42. T. Kinoshita et al., *Appl. Phys. Express*, **5**, 122101 (2012).
43. H. Murotani, D. Akase, K. Anai, Y. Yamada, H. Miyake, and K. Hiramatsu, *Appl. Phys. Lett.*, **101**, 042110 (2012).
44. T. Takano, T. Mino, J. Sakai, N. Noguchi, K. Tsubaki, and H. Hirayama, *Appl. Phys. Express*, **10**, 031002 (2017).
45. K. Ebata, J. Nishinaka, Y. Taniyasu, and K. Kumakura, *Jpn. J. Appl. Phys.*, **57**, 04FH09 (2018).
46. N. Maeda and H. Hirayama, *Phys. Status Solidi (c)*, **10**, 1521 (2013).
47. Y. K. Kuo, J. Y. Chang, F. M. Chen, Y. H. Shih, and H.-T. Chang, "Numerical investigation on the carrier transport characteristics of AlGaN deep-UV light-emitting diodes." *IEEE J. Quantum Electron.*, **52**, 3300105 (2016).
48. J. Zhang, Y. Gao, L. Zhou, Y.-U. Gil, and K.-M. Kim, *Proc. SPIE*, **10940**, 1094002 (2019).
49. J. Zhang, L. Zhou, Y. Gao, A. Lunev, and S. Wu, "Bolb Inc, Livermore CA, U.S. A.UVC LED Lifetime Models and the defect dynamics under stress (private communication)."
50. J. Zhang, Y. Gao, L. Zhou, Y.-U. Gil, and K.-M. Kim, *Semicond. Sci. Technol.*, **33**, 07LT01 (2018).
51. T. Y. Wang, C. T. Tasi, C. Lin, and D. S. Wuu, *Sci. Rep.*, **7**, 14422 (2017).
52. J. Yun and H. Hirayama, *Jpn. J. Appl. Phys.*, **121**, 013105 (2017).
53. S. Y. Karpov and Y. N. Makarov, *Appl. Phys. Lett.*, **81**, 4721 (2002).
54. D. Cameron, P. R. Edwards, F. Mehnke, G. Kusch, L. Sulmoni, M. Schilling, T. Wernicke, M. Kneissl, and R. W. Martin, *Appl. Phys. Lett.*, **120**, 162101 (2022).
55. N. Susilo et al., *Appl. Phys. Lett.*, **112**, 041110 (2018).
56. C.-Y. Huang et al., *AIP Adv.*, **7**, 055110 (2017).
57. A. Fujioka, K. Asada, H. Yamada, T. Ohtsuka, T. Ogawa, T. Kosugi, D. Kishikawa, and T. Mukai, *Semicond. Sci. Technol.*, **29**, 084005 (2014).
58. J. Kim, J. Pyeon, M. Jeon, and O. Nam, *Jpn. J. Appl. Phys.*, **54**, 081001 (2015).
59. T. M. Al Tahtamouni, J. Y. Lin, and H. X. Jiang, *J. Appl. Phys.*, **113**, 123501 (2013).
60. J. Yan, J. Wang, Y. Zhang, P. Cong, L. Sun, Y. Tian, C. Zhao, and J. Li, *J. Cryst. Growth*, **414**, 254 (2015).
61. K. Ding, V. Avrutin, U. Özgür, and H. Morkeç, *Crystals*, **7**, 300 (2017).
62. Z. Bryan, I. Bryan, J. Xie, S. Mita, Z. Sitar, and R. Collazo, *Appl. Phys. Lett.*, **106**, 142107 (2015).
63. T. Nomura, K. Okumura, H. Miyake, K. Hiramatsu, O. Eryu, and Y. Yamada, *J. Cryst. Growth*, **350**, 69 (2012).
64. C. Hartmann, J. Wollweber, S. Sintonen, A. Dittmar, L. Kirste, S. Kollowa, K. Irmscher, and M. Bickermann, *Cryst. Eng. Comm*, **18**, 3488 (2016).
65. C. Reich et al., *Appl. Phys. Lett.*, **107**, 142101 (2015).
66. J. Wang, J. Yan, Y. Guo, Y. Zhang, Y. Tian, S. Zhu, X. Chen, L. Sun, and J. Li, *Sci. Sin. Phys. Mech. Astron.*, **45**, 067303 (2015).
67. S. Inoue, N. Tamari, and M. Taniguchi, *Appl. Phys. Lett.*, **110**, 141106 (2017).
68. J. Lang, F. Xu, W. Ge, B. Liu, N. Zhang, Y. Sun, J. Wang, M. Wang, N. Xie, and X. Fang, *Opt. Express*, **27**, A1458 (2019).
69. D. Lee et al., *Appl. Phys. Lett.*, **110**, 191103 (2017).
70. J. Zheng, S. Li, C. Chou, W. Lin, F. Xun, F. Guo, T. Zheng, S. Li, and J. Kang, *Sci. Rep.*, **5**, 17227 (2015).
71. X. Fan, H. Sun, X. Li, H. Sun, C. Zhang, Z. Zhang, and Z. Guo, *Superlatt. Microstruct.*, **88**, 467 (2015).
72. M. Nakarmi, K. Kim, J. Li, J. Lin, and H. X. Jiang, *H. Appl. Phys. Lett.*, **82**, 3041 (2003).
73. L. Wang, W. He, T. Zheng, Z. Chen, and S. Zheng, *Superlattices Microstruct.*, **133**, 106188 (2019).
74. Z. H. Zhang, S. W. Huang Chen, Y. Zhang, L. Li, S. W. Wang, K. Tian, C. Chu, M. Fang, H. C. Kuo, and W. Bi, *ACS Photonics*, **4**, 1846 (2017).
75. J. Hu, J. Zhang, Y. Zhang, H. Zhang, Q. Long, Q. Chen, M. Shan, S. Du, J. Dai, and C. Chen, *Nanoscale Res. Lett.*, **2019**, 14 (2019).
76. M. Kaneda, C. Pernot, Y. Nagasawa, A. Hirano, M. Ippommatsu, Y. Honda, H. Amano, and I. Akasaki, *Jpn. J. Appl. Phys.*, **56**, 061002 (2017).
77. C. De Santi, M. Meneghini, D. Monti, J. Glaab, M. Guttmann, J. Rass, S. Einfeldt, F. Mehnke, J. Enslin, and T. Wernicke, *Photonics Res.*, **5**, A44 (2017).
78. P. Cantu, S. Keller, U. K. Mishra, and S. P. DenBaars, *Appl. Phys. Lett.*, **82**, 3683 (2003).
79. M. Nakarmi, K. Kim, K. Zhu, J. Lin, and H. X. Jiang, *Appl. Phys. Lett.*, **85**, 3769 (2004).
80. S. Zhu, J. Yan, Y. Zhang, J. Zeng, Z. Si, P. Dong, J. Li, and J. Wang, *Phys. Status Solidi (c)*, **11**, 466 (2014).
81. T. C. Zheng, W. Lin, R. Liu, D. J. Cai, J. C. Li, S. P. Li, and J. Y. Kang, *Sci. Rep.*, **6**, 21897 (2016).
82. A. A. Allerman, M. H. Crawford, M. A. Miller, and S. R. Lee, *J. Cryst. Growth*, **312**, 756 (2010).
83. T. D. Moustakas and R. Paiella, *Rep. Prog. Phys.*, **80**, 106501 (2017).
84. Y. Zhang, S. Krishnamoorthy, J. M. Johnson, F. Akyol, A. Allerman, M. W. Moseley, A. Armstrong, J. Hwang, and S. Rajan, *Appl. Phys. Lett.*, **106**, 141103 (2015).
85. D. Jong Won Lee, J. Yeong Kim, E. Hyuk Park, J. Fred Schubert, J. Kim, Y.-I. Lee, Y. Kim, Park, and Jong Kyu Kim, *Sci. Rep.*, **6**, 22537 (2016).
86. F. Mehnke et al., *Appl. Phys. Lett.*, **105**, 051113 (2014).
87. H. Y. Ryu, I. G. Choi, H. S. Choi, and J. I. Shim, *Appl. Phys. Express*, **6**, 062101 (2013).
88. J. Yun and H. Hirayama, *J. Appl. Phys.*, **121**, 013105 (2017).
89. J. J. Wierer, A. A. Allerman, I. Montaño, and M. W. Moseley, *Appl. Phys. Lett.*, **105**, 061106 (2014).
90. H. Liang et al., *Jpn. J. Appl. Phys.*, **55**, 031202 (2016).
91. T. Inazu et al., *Jpn. J. Appl. Phys.*, **50**, 122101 (2011).
92. S. Teramura, Y. Kawase, Y. Sakuragi, S. Iwayama, M. Iwaya, T. Takeuchi, S. Kamiyama, I. Akasaki, and H. Miyake, *Phys. Status Solidi A*, **217**, 1900868 (2020).
93. Y. Kashima et al., *Appl. Phys. Express*, **11**, 012101 (2018).
94. T. C. Zheng, W. Lin, R. Liu, D. J. Cai, J. C. Li, S. P. Li, and J. Y. Kang, *Scientific Rep.*, **6**, 21897 (2016).
95. K. Mori, K. Takeda, T. Kusafuka, M. Iwaya, T. Takeuchi, S. Kamiyama, I. Akasaki, and H. Amano, *Jpn. J. Appl. Phys.*, **55**, 05FL03 (2016).
96. H. Long, S. Wang, J. Dai, F. Wu, J. Zhang, J. Chen, R. Liang, Z. C. Feng, and C. Chen, *Opt. Express*, **26**, 680 (2018).
97. N. Trivellin, D. Fiorimonte, F. Piva, M. Buffolo, C. D. Santi, G. Meneghesso, E. Zanoni, and M. Meneghini, *Electronics*, **11**, 728 (2022).
98. J. Glaab et al., *J. Appl. Phys.*, **123**, 104502 (2018).
99. R. Gaska, *MRS Proc.*, **64**, C6 (2003), 9.
100. H. Amano et al., *J. Phys. D Appl. Phys D: Applied Physics*, **53**, 503001 (2020).
101. F. Rossi et al., *J. Appl. Phys.*, **99**, 053104 (2006).
102. M. Meneghini, A. Tazzoli, G. Mura, G. Meneghesso, and E. Zanoni, *IEEE Trans. Electron Devices*, **57**, 108 (2010).
103. X. A. Cao, P. M. Sandvik, S. F. LeBoeuf, and S. D. Arthur, *Microelectron. Reliab.*, **43**, 1987 (2003).
104. S. W. Lee et al., *Appl. Phys. Lett.*, **89**, 132117 (2006).
105. K. Orita, M. Meneghini, H. Ohno, N. Trivellin, N. Ikedo, S. Takigawa, M. Yuri, T. Tanaka, E. Zanoni, and G. Meneghesso, *IEEE J. Quantum Electron.*, **48**, 1169 (2012).
106. E. Kioupakis, Q. Yan, D. Steiauf, and C. G. Van de Walle, *New J. Phys.*, **15**, 125006 (2013).
107. Y.-Z. Wang et al., *Appl. Phys. Lett.*, **116**, 203501 (2020).
108. S. Sawyer, S. L. Rumyantsev, and M. S. Shur, *Solid-State Electronics*, **52**, 968 (2008).
109. C. G. Moe et al., *Appl. Phys. Lett.*, **96**, 213512 (2010).
110. M. L. Nakarmi, N. Nepal, J. Y. Lin, and H. X. Jiang, *Appl. Phys. Lett.*, **94**, 091903 (2009).
111. A. Pinos, S. Marcinkevičius, J. Yang, R. Gaska, M. Shatalov, and M. S. Shur, *J. Appl. Phys.*, **108**, 093113 (2010).
112. A. Pinos, S. Marcinkevičius, and M. S. Shur, *J. Appl. Phys.*, **109**, 103108 (2011).
113. M. Su, X. Zhu, Q. Guo, Z. Chen, S. Deng, Z. Chen, Y. Wang, J. Deng, and W. Sun, *AIP Adv.*, **11**, 035315 (2021).
114. J. Glaab, J. Ruschel, F. Mehnke, M. Lapeyrade, M. Guttmann, T. Wernicke, M. Weyers, S. Einfeldt, and M. Kneissl, *Semicond. Sci. Technol.*, **33**, 095017 (2018).
115. Z. Ma, H. Cao, S. Lin, X. Li, and L. Zhao, *Solid-State Electron.*, **156**, 92 (2019).
116. K. Ban, J.-ichi Yamamoto, K. Takeda, K. Ide, M. Iwaya, T. Takeuchi, S. Kamiyama, I. Akasaki, and H. Amano, *Appl. Phys. Express*, **4**, 052101 (2011).
117. A. Knauer et al., *J. Appl. Phys.*, **58**, SCCC02 (2019).
118. A. Y. Polyakov and I.-H. Lee, *Mater. Sci. Eng. R*, **94**, 1 (2015).
119. A. Y. Polyakov, N. B. Smirnov, and A. V. Govorkov, *J. Appl. Phys.*, **91**, 5203 (2002).
120. H. Zhang, W. Zhang, S. Zhang, M. Shan, Z. Zheng, A. Wang, L. Xu, F. Wu, J. Dai, and C. Chen, *IEEE Electron Dev. Lett.*, **42**, 978 (2021).
121. C. C. Lu, C. P. Wang, C. Y. Liu, and C. P. Hsu, *IEEE Trans. Electron Dev.*, **2016**, 3143 (2016).
122. A. Uedono et al., *J. Appl. Phys.*, **105**, 054501 (2009).
123. J. Ruschel, J. Glaab, B. Beidoun, N. L. Ploch, J. Rass, T. Kolbe, A. Knauer, M. Weyers, S. Einfeldt, and M. Kneissl, *Photon. Res.*, **7**, B36 (2019).
124. J. Ruschel et al., *J. Appl. Phys.*, **124**, 084504 (2018).
125. J. Glaab et al., *IEEE Photon. Technol. Lett.*, **31**, 529 (2019).
126. D. Monti et al., *IEEE Trans Electron Dev*, **66**, 3387 (2017).
127. N. Trivellin, D. Monti, C. DeSanti, M. Buffolo, G. Meneghesso, E. Zanoni, and M. Meneghini, *Microelectron Rel*, **88-90**, 868 (2018).
128. M. H. Chang, D. Das, P. Varde, and M. Pecht, *Microelectron. Reliab.*, **52**, 762 (2012).
129. C. Y. Huang, P. Y. Wu, K. S. Chang, Y. H. Lin, W. C. Peng, Y. Y. Chang, J. P. Li, H. W. Yen, Y. S. Wu, and H. Miyake, *AIP Adv.*, **7**, 055110 (2017).
130. S. Walde, S. Hagedorn, P. M. Coulon, A. Mogilatenko, C. Netzel, J. Weinrich, N. Susilo, E. Ziffer, L. Matiwe, and C. Hartmann, *J. Cryst. Growth*, **531**, 125343 (2020).
131. H. Sun, S. Mitra, R. C. Subedi, Y. Zhang, W. Guo, J. Ye, M. K. Shakfa, T. K. Ng, B. S. Ooi, and I. S. Roqan, *Adv. Funct. Mater.*, **29**, 1905445 (2019).
132. K. Uesugi, K. Shojiki, Y. Tezen, Y. Hayashi, and H. Miyake, *Appl. Phys. Lett.*, **116**, 062101 (2020).
133. N. Susilo, E. Ziffer, S. Hagedorn, L. Cancellara, C. Netzel, N. L. Ploch, S. Wu, J. Rass, J. S. Walde, and L. Sulmoni, *Photonics Res.*, **2020**, 589 (2020).
134. Y. Zhang, H. Long, J. Zhang, B. Tan, Q. Chen, S. Zhang, M. Shan, Z. Zheng, J. Dai, and C. Chen, *Cryst. Eng. Comm*, **21**, 4072 (2019).
135. J. Glaab et al., *J. Appl. Phys.*, **131**, 014501 (2022).
136. V. Adivarahan, W. H. Sun, A. Chitnis, M. Shatalov, S. Wu, H. P. Maruska, and M. A. Khan, *Appl. Phys. Lett.*, **85**, 2175 (2004).
137. M. Meneghini, D. Barbisan, L. Rodighiero, G. Meneghesso, and E. Zanoni, *Appl. Phys. Lett.*, **97**, 143506 (2010).
138. N. Trivellin, D. Monti, F. Piva, M. Buffolo, C. Santi, E. Zanoni, G. Meneghesso, and M. Meneghini, *Japanese J. Appl. Phys*, **58**, SCCC19 (2019).
139. C. Sah, R. N. Noyce, and W. Shockley, *Proc. IRE*, **45**, 1228 (1957).

140. H. Masui, *Semicon. Sci. Technol*, **26**, 075011 (2011).
141. J. M. Shah, Y.-L. Li, T. Gessmann, and E. F. Schubert, *J. Appl. Phys.*, **94**, 2627 (2003).
142. H. Masui, S. Nakamura, and S. P. DenBaars, *Appl. Phys. Lett.*, **96**, 073509 (2010).
143. M. Meneghini, F. Piva, C. D. Santi, N. Trivellin, and M. Buffolo, *Proc. SPIE*, **12001**, 120010B (2022).
144. T. S.-C. Hsu et al., *Photonics*, **8**, 196 (2021).
145. Y. Kawase, S. Ikeda, Y. Sakuragi, S. Yasue, S. Iwayama, M. Iwaya, T. Takeuchi, S. Kamiyama, I. Akasaki, and H. Miyake, *Jpn. J. Appl. Phys.*, **58**, SC1052 (2019).
146. X. Yang, B. Sun, Z. Wang, C. Qian, Y. Ren, D. Yang, and Q. Feng, *Materials*, **11**, 817 (2018).
147. M. Su, H. Liu, M. Cai, and W. Sun, *IEEE Trans. Electron. Dev.*, **70**, 570 (2023).
148. H. Kobayashi, K. Sato, Y. Okuaki, T. G. Lee, T. Morishita, H. Goto, and N. Kuze, *Appl. Phys. Lett.*, **122**, 101103 (2023).
149. N. Roccato et al., *Appl. Phys. Lett.*, **122**, 161105 (2023).
150. L. Schowalter, (2020).
151. C. Qian, J. J. Fan, J. Fang, C. Yu, Y. Ren, X. J. Fan, and G. Q. Zhang, *Materials*, **10**, 1181 (2017).
152. M. Fukuda, *Reliability and Degradation of Semiconductor Lasers and LEDs* (Artech House, Boston) (1991).
153. J. J. Fan, C. Qian, K. C. Yung, X. J. Fan, G. Q. Zhang, and M. Pecht, *IEEE Trans. Device Mater. Reliab.*, **15**, 576 (2015).
154. B. Sun, X. P. Jiang, K. C. Yung, J. J. Fan, and M. Pecht, *IEEE Trans. Power Electron.*, **32**, 6338 (2017).
155. IES-LM-80-08, *Approved Method for Lumen Maintenance Testing of LED Light Source* (Illuminating Engineering Society, New York, NY, USA) (2008).
156. IES-TM-21-11, *Projecting Long Term Lumen Maintenance of LED Light Sources* (Illuminating Engineering Society, New York, NY, USA) (2011).
157. J. L. Huang, D. S. Golubović, S. Koh, D. G. Yang, X. P. Li, X. J. Fan, and G. Q. Zhang, *Opt. Express*, **23**, A966 (2015).
158. J. J. Fan, K. C. Yung, and M. Pecht, *IEEE Trans. Device Mater. Reliab.*, **12**, 470 (2012).
159. B. Sun, X. J. Fan, H. Y. Ye, J. J. Fan, C. Qian, W. D. Van Driel, and G. Q. Zhang, *Reliab. Eng. Syst. Saf.*, **163**, 14 (2017).
160. J. Huang, D. S. Golubovic, S. Koh, D. Yang, X. Li, X. Fan, and G. Q. Zhang, *Reliab. Eng. Syst. Saf.*, **154**, 152 (2016).
161. D. Han, *Reliab. Eng. Syst. Saf.*, **140**, 1 (2015).
162. E. M. Benavides, *IEEE Trans. Reliab.*, **60**, 219 (2011).
163. B. Hamon and W. D. van Driel, *Microelectron. Reliab.*, **64**, 599 (2016).
164. M. Y. Mehr, W. D. Van Driel, and G. Q. Zhang, *J. Electron. Mater.*, **2016**, 444 (2016).
165. C. Qian, X. J. Fan, J. J. Fan, C. A. Yuan, and G. Q. Zhang, *Reliab. Eng. Syst. Saf.*, **147**, 84 (2016).
166. L. Trevisanello, M. Meneghini, G. Mura, M. Vanzi, M. Pavesi, G. Meneghesso, and E. Zanoni, *IEEE Trans. Device Mater. Reliab.*, **8**, 304 (2008).
167. X. B. Luo, B. L. Wu, and S. Liu, *IEEE Trans. Dev. Mater. Reliab.*, **10**, 182 (2010).
168. T. Yanagisawa and T. Kojima, *J. Lumines.*, **114**, 39 (2005).
169. J. Huang, D. S. Golubović, S. Koh, D. Yang, X. Li, X. J. Fan, and G. Q. Zhang, *IEEE Trans. Device Mater. Reliab.*, **15**, 478 (2015).
170. J. Huang, D. S. Golubović, S. Koh, D. Yang, X. Li, X. J. Fan, and G. Q. Zhang, *IEEE Trans. Device Mater. Reliab.*, **15**, 220 (2015).
171. M. Vázquez, N. Núñez, E. Nogueira, and A. Borreguero, *Microelectron. Reliab.*, **50**, 1559 (2015).
172. M. Edirisinghe and P. Rathnayake, *Int. Lett. Chem. Phys. Astron.*, **49**, 48 (2015).
173. Y. H. Yang, Y. F. Su, and K. N. Chiang, "Acceleration factor analysis of aging test on gallium nitride (GaN)-based high power light-emitting diode (LED)." *Proc. Thermal and Thermomechanical Phenomena in Electronic Systems*, Orlando, FL, USA (2014).
174. F. Piva, C. De Santi, M. Deki, M. Kushimoto, H. Amano, H. Tomozawa, N. Shibata, G. Meneghesso, E. Zanoni, and M. Meneghini, *Photon. Res.*, **8**, 1786 (2020).
175. F. P. Nicola Trivellin, C. D. S. Matteo Buffolo, G. M. Enrico Zanoni, and M. Meneghini, "UVC LED reliability and its effect on disinfection systems design." *Proc. SPIE 12441, Light-Emitting Devices, Materials, and Applications XXVII*, **1244103** (2023).
176. L. Z. Jianping Zhang, A. L. Ying Gao, B. Z. Shuai Wu, and A. Werner Götz, *Phys. Lett.*, **122**, 101106 (2023).
177. L. Liu, M. Ling, J. Yang, W. Xiong, W. Jia, and G. Wang, *J. Appl. Phys.*, **111**, 093110 (2012).
178. J. Zhang, L. Zhou, Y. Gao, A. Lunev, B. Zhang, and W. Götz, *Semicond. Sci. Technol.*, **37**, 07LT01 (2022).
179. J. Zhang, L. Zhou, Y. Gao, A. Lunev, B. Zhang, and S. Wu, *Phys. Status Solidi*, A 2200433 (2023).
180. M. Buffolo, A. Caria, F. Piva, N. Roccato, C. Casu, C. De Santi, N. Trivellin, G. Meneghesso, E. Zanoni, and M. Meneghini, *Phys.Status Solidi A*, **219**, 2100727 (2022).
181. M. A. Hopkins, D. W. E. Allsopp, M. J. Kappers, R. A. Oliver, and C. J. Humphreys, *J. Appl. Phys.*, **122**, 234505 (2017).
182. R. D. Tobias, An introduction to partial least squares regression,' 1996. MathWorks. (2022) Partial least squares regression and principal components regression. [Online]. Available:(https://mathworks.com/help/stats/ partial-least-squares-regression-and-principal-components-regression.html).
183. C. J. Zollner, S. P. DenBaars, J. S. Speck, and S. Nakamura, *Semicond. Sci. Technol.*, **36**, 123001 (2021).
184. S. Karpov, *Opt. Quantum Electron.*, **47**, 1293 (2015).
185. J. Shim and D. Shin, *Nanophotonics*, **7**, 1601 (2018).
186. Q. Dai et al., *Microelectron. Reliab.*, **78**, 46 (2017).
187. X. Qu, H. Wang, X. Zhan, F. Blaabjerg, and H. S. H. Chung, *IEEE Trans. Power Electron.*, 2017**32**, 8718 (2017).
188. B. C. Letson, "Assessment and enhancement of deep UV LED reliability for long duration space mission." *PhD Dissertation*, University of Florida (2022).
189. B. C. Letson, S. Barke, P. Wass, G. Mueller, F. Ren, S. J. Pearton, and J. W. Conklin, *J. Vac. Sci. Technol. A*, **41**, 013202 (2023).
190. B. C. Letson, S. Barke, S. P. Kenyon, T. Olatunde, G. Mueller, P. Wass, F. Ren, S. J. Pearton, and J. W. Conklin, *Rev. Sci. Instrum.*, **93**, 114503 (2022).
191. F. Piva et al., *Appl. Phys. Lett.*, **122**, 151108 (2023).
192. M. Buffolo, A. Caria, F. Piva, N. Roccato, C. Casu, C. De Santi, N. Trivellin, G. Meneghesso, E. Zanoni, and M. Meneghini, *, Physica Status Solidi (a)*, **219**, 2100727 (2022).
193. F. Ren, C. R. Abernathy, S. N. G. Chu, J. R. Lothian, and S. J. Pearton, *Solid-State Electron.*, **38**, 1137 (1995).
194. F. K. Wang and T. P. Chu, *Microelectron. Reliab.*, **52**, 1332 (2012).
195. E. Nogueira and J. Mateos, "Accelerated life testing LEDs on temperature and current." *Proceedings of the Electron Devices (CDE)*, Palma de Mallorca, Spain (2011).